AD-A069 883 VON KARMAN INST FOR FLUID DYNAMICS RHODE-SAINT-GENESE--ETC F/G 20/4
HEAT TRANSFER AND PRESSURE MEASUREMENT ON A CONCAVE CONIC MODEL--ETC(U)
NOV 78 B E RICHARDS AFOSR-78-3474

UNCLASSIFIED VKI-INTERNAL NOTE-61 AFOSR-TR-79-0658 NL

| OF |
AD
A069883

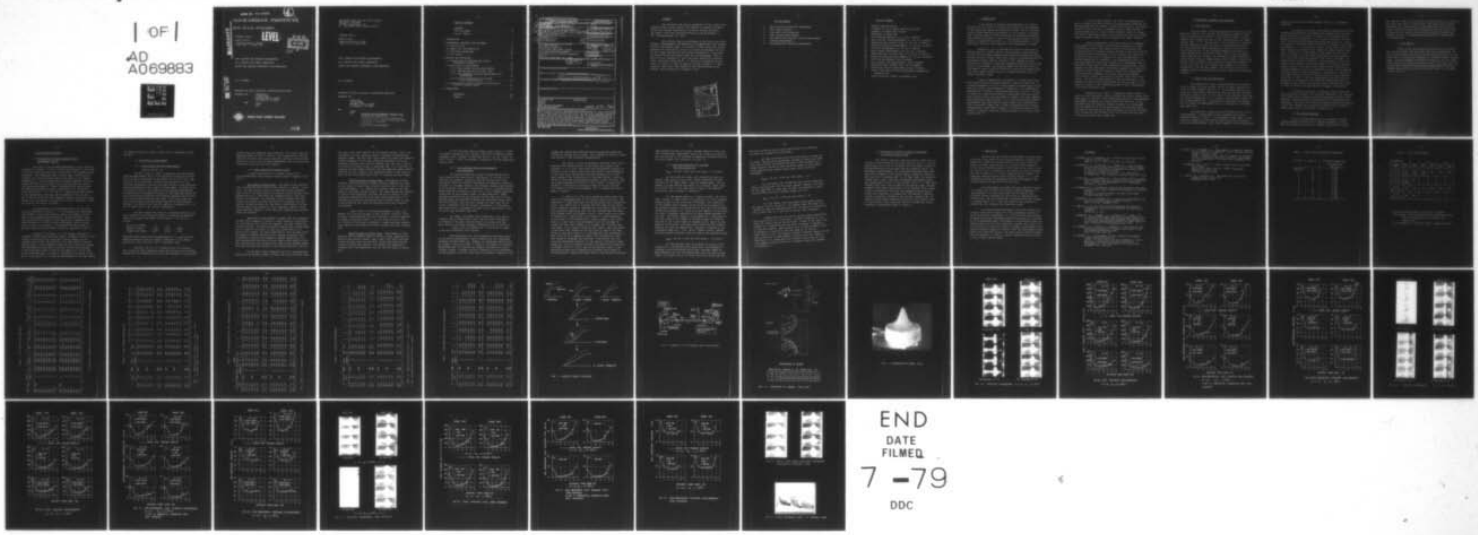

END
DATE
FILMED
7 -79
DDC

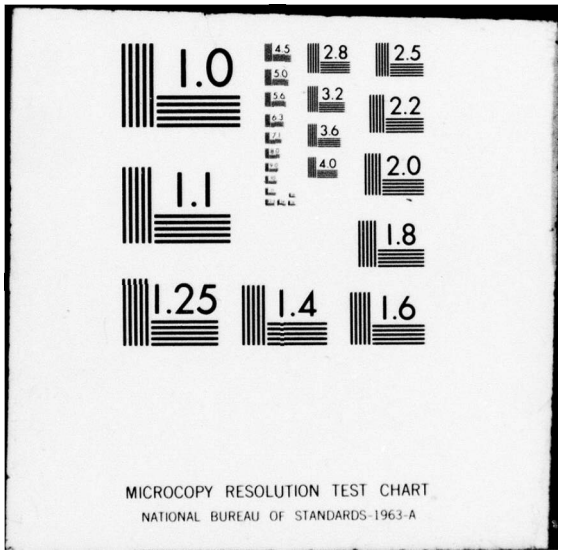
1.0
1.1
1.25
1.4
1.6
1.8
2.0
2.2
2.5
2.8
3.2
3.6
4.0
4.5
5.0
5.6
6.3
MICROCOPY RESOLUTION TEST CHART
NATIONAL BUREAU OF STANDARDS-1963-A

# von KARMAN INSTITUTE

## FOR FLUID DYNAMICS



LEVEL II

INTERNAL NOTE 61

AFOSR 78-3474

INTERIM SCIENTIFIC REPORT
1 DEC 1977 - 30 NOV 1978



# *HEAT TRANSFER AND PRESSURE MEASUREMENTS ON A CONCAVE CONIC MODEL UNDER BOTH STEADY AND UNSTEADY HYPERSONIC FLOW CONDITIONS*



B.E. RICHARDS



PREPARED FOR : SAMSO/RSSE
PO BOX 92960
WORLDWAY POSTAL CENTER
LOS ANGELES, CA 90009

AND EOARD
FPO

RHODE SAINT GENESE BELGIUM

VON KARMAN INSTITUTE FOR FLUID DYNAMICS
AEROSPACE DEPARTMENT
CHAUSSEE DE WATERLOO, 72
B - 1640 RHODE SAINT GENESE, BELGIUM

INTERNAL NOTE 61

AFOSR 78-3474

INTERIM SCIENTIFIC REPORT
1 DEC 1977 - 30 NOV 1978

# *HEAT TRANSFER AND PRESSURE MEASUREMENTS ON A CONCAVE CONIC MODEL UNDER BOTH STEADY AND UNSTEADY HYPERSONIC FLOW CONDITIONS*

B.E. RICHARDS



PREPARED FOR :

SAMSO/RSSE
PO BOX 92960
WORLDWAY POSTAL CENTER
LOS ANGELES, CA 90009

AND

EOARD
FPO

TABLE OF CONTENTS

UNCLASSIFIED

SECURITY CLASSIFICATION OF THIS PAGE *(When Data Entered)*

| REPORT DOCUMENTATION PAGE | READ INSTRUCTIONS BEFORE COMPLETING FORM |
|---|---|
| 1. REPORT NUMBER: AFOSR-TR-79-0658 | 2. GOVT ACCESSION NO. / 3. RECIPIENT'S CATALOG NUMBER |
| 4. TITLE (and Subtitle): HEAT TRANSFER AND PRESSURE MEASUREMENT ON A CONCAVE CONIC MODEL UNDER BOTH STEADY AND UNSTEADY HYPERSONIC FLOW CONDITIONS | 5. TYPE OF REPORT & PERIOD COVERED: INTERIM rept. 1 Dec 77 - 30 Nov 78 |
| | 6. PERFORMING ORG. REPORT NUMBER: VKI Internal Note 61 |
| 7. AUTHOR(s): BRYAN E. RICHARDS | 8. CONTRACT OR GRANT NUMBER(s): AFOSR-78-3474 |
| 9. PERFORMING ORGANIZATION NAME AND ADDRESS: VON KARMAN INSTITUTE, CHAUSSEE DE WATERLOO, 72, B-1640 RHODE SAINT GENESE, BELGIUM | 10. PROGRAM ELEMENT, PROJECT, TASK AREA & WORK UNIT NUMBERS: 2307A1, 61102F, A1 |
| 11. CONTROLLING OFFICE NAME AND ADDRESS: AIR FORCE OFFICE OF SCIENTIFIC RESEARCH/NA, BLDG 410, BOLLING AIR FORCE BASE, D C 20332 | 12. REPORT DATE: Nov 78 |
| | 13. NUMBER OF PAGES: 45 |
| 14. MONITORING AGENCY NAME & ADDRESS *(if different from Controlling Office)* | 15. SECURITY CLASS. *(of this report)*: UNCLASSIFIED |
| | 15a. DECLASSIFICATION/DOWNGRADING SCHEDULE |

16. DISTRIBUTION STATEMENT *(of this Report)*

Approved for public release; distribution unlimited.

VKI-INTERNAL NOTE-61

17. DISTRIBUTION STATEMENT *(of the abstract entered in Block 20, if different from Report)*

18. SUPPLEMENTARY NOTES

19. KEY WORDS *(Continue on reverse side if necessary and identify by block number)*

HYPERSONIC FLOW
REENTRY
MISSILE
HEAT TRANSFER MEASUREMENTS
PRESSURE MEASUREMENTS
UNSTEADY FLOW

411 190

20. ABSTRACT *(Continue on reverse side if necessary and identify by block number)*

Heat transfer and pressure measurements have been measured on a conic configuration w th a strongly concave surface and a blunt nose tip in the von Karman Institute Longshot free piston tunnel at M-15 and 20. The test flow parameters achieved closely simulated reentry aerodynamic conditions. Information derived from the measurements and also from high speed cine schlieren sequences enabled information to be derived on the effect of Mach number, Reynolds number, surface roughness and flow incidence on the flow over the model, the heat transfer distribution and stability of the flow.

DD FORM 1 JAN 73 1473

UNCLASSIFIED

SECURITY CLASSIFICATION OF THIS PAGE *(When Data Entered)*

FOREWORD

The activities and results documented in this report were supported under Project 63311F with Captain R. Chambers of Space and Missile Systems Organization, acting as project engineers. The report covers work conducted during the period December 1, 1977 through November 30, 1978.

The technical advice and guidance by Mr Victor DiCristina, Manager, Thermodynamics and Materials Test Department, Avco Systems Division, Wilmington, Mass. in the area of model design and instrumentation was particularly value. The author acknowledges the help of Mssrs Roger Conniasselle and Fernand Vandenbroeck in operating the tunnel and Mr Jean-Claude Lobet for the photography. Mssrs B. Boussin and D. Desnoyer of Ecole Nationale Supérieure d'Aéronautique, Toulouse, France and Mr. P. Phlips of Southampton University, U.K. and Mr C. Beer of Imperial College, London, U.K. participated in the tests, data reduction and interpretation of the results, while carrying out "stages" at VKI.

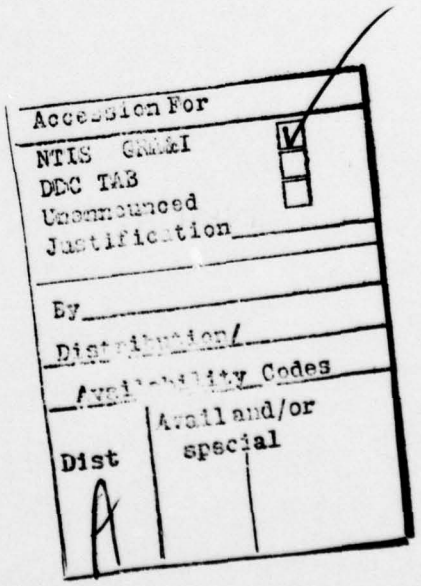

## LIST OF TABLES

## LIST OF FIGURES

## 1. INTRODUCTION

In the design of ablation type components for reentry vehicles, it is critical to be able to predict the flow behaviour on the complicated shapes evolved during flight. The full problem involves understanding the processes in, for instance, a boundary layer with mass addition from ablation with transition and maybe flow instability present. A useful input can be obtained from the testing of appropriate passive, i.e., non ablating models in flow conditions similar to that expected to be encountered in flight.

Because of lack of advanced facilities in operation at present, and for economic reasons, most parametric test programs are carried out at Mach numbers much below that encountered during the most critical reentry region with regard to maximum deceleration and maximum surface heating. Studies in the Longshot facility, described in reference 1, have the advantage that mainly exact simulation of Mach number and Reynolds number are achieved with full size models. Hence, using this facility, checks can be made on the lower Mach number studies as well as pinpointing other areas of further necessary study.

Figure 1 demonstrates the families of shapes which have been found on ablating reentry nosetips. Studies to date have included measurements on 50°-8° biconic models (representing a "blunt turbulent shape") and hemispheres ("spherical"). The experimental measurements in laminar, transitional,turbulent flow on a variety of smooth and rough-walled models of these types with and without nose bluntness and at various angles of attack, have been compared with appropriate theories (Refs. 2, 3). Pressure and heat transfer measurements have been made on convex shapes (also representing "blunt turbulent" shapes, Ref. 4) and on concave biconic surfaces (representing "transitional" shapes). A preliminary phase of the study of "unsteady" flows over concave shapes has also been accomplished (Ref. 5).

In all of these studies, the level of achievement has been in checking the feasibility of the measurement technique and to developing initial analyses to explain the results. The present series of tests involves a systematic study of the flow over a concave shape which is close to the "unsteady" family of shapes. The study in particular deals with the effect on the flow of Mach number, Reynolds number, surface roughness and model incidence.

Surface indentation in the nose region of axisymmetric blunt bodies in high speed flow has been considered as a means of decreasing drag in high speed cruise or glide vehicles and increasing drag in planetary reentry vehicles as well as occurring on ablating missile nose-cones. For this reason the subject has attracted a great deal of interest. For some configurations of surface indentation or concavity, flow unsteadiness occurs. The most comprehensive study made to date on this phenomenon (Ref. 6) identifies three types of flow unsteadiness ranging from : small movements of the shock waves induced by unsteady small separated regions (called "vibration" mode of instability); unsteadiness involving larger movements of the bow shock was designated "oscillation"; and an explosive but periodic flow called "pulsation". The most striking feature of the pulsation mode is the movement of the bow shock wave between the two extremes as illustrated in figure 1. The information gained in this study appears to be mainly pulsation flow.

Kenworthy et al. (Ref. 7) reported a study to gain insight into the "pulsation" mode of instability using a spiked blunt body shape in a Mach 6.0 flow through application of time-dependent measurement techniques and simple shock-polar analyses. It was concluded that the unusually intense instability is associated with the formation of a high speed annular jet directed towards the root of the spike due to the interaction of the weak foreshock and a strong aft shock present for a little more than one tenth of the cycle time of the instability.

## 2. EXPERIMENTAL APPARATUS AND PROCEDURE

### 2.1 Test facility

The von Karman Institute Longshot test facility as schematized in figure 2 was used for this program. Longshot differs from a conventional gun tunnel in that a heavy piston is used to compress the nitrogen test gas to very high pressures and temperatures (Refs. 1, 3). The test gas is then trapped in a reservoir at peak conditions by the closing of a system of check valves. The flow conditions decay monotonically during 10 to 20 millisecond running times as the nitrogen trapped in the reservoir flows through the 6° half-angle conical nozzle into the preevacuated open jet test chamber. The extremes in supply conditions used in these tests are approximately 55,000 $lb/in^2$ at 1900°K and 38,000 $lb/in^2$ at 2320°K. These provide unit Reynolds numbers of $8.5\times10^6$ and $2\times10^6$ per ft at nominal Mach numbers of 15 and 20, respectively. The two Mach numbers were obtained at the 14 in. diameter nozzle exit plane by using throat inserts with different diameters.

### 2.2 Models and instrumentation

The concave conic model designated Model M was supplied by Avco Systems Division and had a 0.437 in radius nosetip and a 7.294 in. base diameter (see Fig. 3). The forebody consisted initially of a cone with an angle of 22° up until the model diameter achieved a value of 2.15 in. The radius of the generator defining the convex forebody was 2.5 in. giving a surface angle change from 22° to approximately 85°. The shoulder of the model was rounded off to a radius of approximately 0.4 in. leading to an afterbody cone angle of 6°.

The model was tested with two different levels of surface roughness. A sandblasted surface roughness with a mean roughness height of 0.005 in. is designated as model MR1. A larger scale of roughness was achieved by bonding spherical aluminium particles to the surface. This larger roughness scale configuration

using a particle size of mean diameter 0.065 in. is designated model MR2.

Ten copper calorimeter heat transfer gauges manufactured by BBN and supplied with the models were mounted flush along the model surface as illustrated in figure 2. The locations of the gauges have been designated A to J in order of distance from the nose. The heat transfer gauges mounted at positions B, D, F and I are located on the upper side of the model as mounted in the tunnel and gauges A, C, E, G and B are located on the lower side of the model. Gauge H is located at 30° around the model from the lower side. The distance of the center of each gauge from the nose is given in figure 3. An additional gauge which has been contoured to fit the local shape was placed on the nose of the model. Ten pressure taps located at stations A-J were mounted at positions diametrically opposite (except for gauge H) to the heat transfer gauges. Details of the heat sensors used and the associated recording equipment is given in references 8 and 9. The calibration technique used for these transducers is described in reference 4. The gauge calibration factors found and used for data reduction are given in Table 1. Pressure measurements were made using PCB piezoelectric transducers. This method of measuring pressures is standard in the Longshot testing. No special measures were taken in order to measure the expected high frequency fluctuations.

The reservoir pressure is measured using Kistler Type 6201 piezoelectric gauges. The reservoir temperature was assessed from signals from a tungsten-rhenium thermocouple mounted in the reservoir. Pitot pressures are measured with a PCB piezoelectric transducer. The tunnel test flow has undergone detailed calibration at the four standard test conditions using fine wire stagnation temperature probes as described in reference 10.

## 2.3 Schlieren photography

An 18 in conventional single pass Toepler schlieren system equipped with high quality optical components is used. With the exception of one 24 in. diameter plane mirror to bend

the light 90° (due to the vicinity of a wall near the test section) the light beam takes a Z-shaped path. High speed ciné schlieren photographs were taken using a 16 mm Kodak ciné camera. Framing rates of 6,000 per second were achieved during the running time by operating the camera without the rotating prism shutter and exposing the film to sequenced multiple sparks of approximately 1 μsec duration.

## 2.4 Test matrix

Table 2 gives the scope of the test series and identifies the test number with each model and flow configuration. It can be seen that the test series provides cross sections of a complete matrix involving the parameters of flow Mach number, Reynolds number, surface roughness and angle of incidence. The test conditions given in this table are nominal values. The actual test conditions were calculated from appropriate measurements using the Longshot data reduction program (described in Ref. 8) and summarized in Table 3.

## 3. RESULTS AND DISCUSSION

### 3.1 Presentation of time-averaged results and general remarks

The overall time averaged measurements of the study are presented in figures 5, 6 and 7. These are displayed in such a way as to facilitate the discussion of the effects of changing various parameters. The dimensional heat transfer rate, normalized heat transfer rate and normalized pressure are given in the figures designated b, c and d, respectively. Selected sequences of photographs from the ciné schlieren flow visualizations are given in the figures designated a. Figure 5 represents the results taken on models MR1 and MR2 at nominal conditions of M = 16 and Re = $9\times10^6$ per foot at $\alpha$ = 0°, +3° and -3°. Figure 6 gives the results on the same models and at the same incidences at M = 20, and Re = $3\times10^6$ per foot. The final figure 7 presents results on these models at M = 16 and Re = $4.5\times10^6$ per ft and M = 20 and Re = $2\times10^6$ per foot at zero angles of attack.

The experimental and normalized results for all tests are also presented in Tables 4 - 7. The pressures are normalized with respect to the pitot pressure, which is assumed to be the same as the stagnation point pressure. The heat transfer rates are normalized with respect to the theoretical stagnation point heat transfer on a 0.437 in. radius hemisphere, whose value is given in Table 3, and which is calculated from free stream conditions using the Fay and Riddel formula as presented in Ref. 8.

A negative incidence, $\alpha$, in the figures represents a "leeward" surface, and a positive value a "windward" surface. Since during one particular test some heat transfer gauges are on a windward surface when the pressure at the same distance from the leading edge is on the leeward surface and vice versa, the figures are rearranged to align data on surfaces with the same attitude to the flow rather than in terms of run numbers (as in the case of the tabulated data). In order to interpret the location of the data, in the tables "t" is used for measurements on the top surface,

"b" denotes bottom (or lower) surface and "s" represents a side position.

### 3.2 Discussion of measurements

#### 3.2.1 Time-averaged pressure measurements

(Figures 5d, 6d, 7d)

For the 0° and -3° cases, in general, the time-averaged pressure measurements show a flat pressure distribution with distance sensed by the gauges in the region of 1.5 to 4.5 ins. from the nose. This observation, backed up by examination of the schlieren photographs indicate that there exists a large separated region extending over this range for these angle of attack cases. The pressure level in this region can be assessed approximately by guessing the displacement thickness of the separated region and then calculating the pressure distribution assuming inviscid flow over the resultant effective body shape. If we assume that the shear layer extends from the nosetip shoulder to the afterbody shoulder, its angle to the flow for angles of incidence of -3°, 0° and +3° would be 37°, 40° and 43° respectively.

For these angles the pressure non-dimensionalized by the pitot pressure in the separated region as predicted by Newtonian theory and tangent cone theory in the range $15 < M < 20$ is as follows

| Angle of incidence | -3° | 0° | 3° |
|---|---|---|---|
| Newtonian theory | 0.362 | 0.413 | 0.465 |
| Tangent cone theory | 0.417 | 0.476 | 0.537 |

Comparing these values with the measurements it is seen that the measured pressure levels are roughly predicted by this simple analysis at least for the 0° and -3° incidence cases.

Generally, for the +3° incidence cases, the pressure falls below the above tabulated values near the nose, but increases rapidly over the remaining position of the forebody to values often

greater than the stagnation point pressure. This arises since the separated region of flow is smaller, the intersection of the bow shock and aft shock wave occurs above the surface in front of the shoulder as seen in the schlieren photographs, with the resulting interaction occurring near the shoulder.

### 3.2.2 Time-average heat transfer rates

In these discussions it is chosen to make use of the non-dimensional heat transfer results given in figures 5c, 6c and 7c.

Zero angle of attack cases : The shape of the distribution of normalized heat transfer with distance is similar in all cases. The heat transfer drops to around 20% of the stagnation point value at the beginning of the concave surface and then rises monotonically to a value above the stagnation point value just ahead of the shoulder. The increase in heat transfer rate with distance in regions in which the pressure is constant over the concave surface indicates that the flow is transitional. (If the flow had been fully laminar, or fully turbulent, then for these large separated regions it would have been expected that constant heating be present).

Comparison of measurements on models MR1 (low roughness) and MR2 (high roughness) indicate a slight lowering in heat transfer distribution with increasing roughness. No other information on heating within extensive separation regions with surface roughness is known to the author to check this observation. It is pointed out, however, for these rough models, that the heat transter gauges lie below the mean surface and may be sensing local interactions caused by the roughness elements themselves. It is thus expected that the results on the rough surface model will be more scattered and less accurate than those on the smoother models. This must be taken into account in the interpretation of the data.

For the same surface roughness case it is observed that decreasing the Reynolds number decreases the normalized heat trans-

fer rate on the later sections of the concave surface. This is an indication that the transition point is delayed with decreasing Reynolds number. The fact that little effect was found with changing surface roughness for the same conditions mentioned in the last paragraph indicates that surface roughness does not play a role in the transition process within a separated flow. It is difficult to separate the Mach number behaviour from the Reynolds number behaviour mentioned earlier. However, the impression given is that there appears to be little significant effect of changing the Mach number.

Positive angle of attack cases : Measurements of heat transfer on positive angle of attack surfaces compared with those at zero angle of attack show a similar trend to that in the pressure measurements, i.e., higher heat transfer rates on the later stages of the model concave surface. This again denotes the presence of earlier flow separation and hence the earlier effects of the interaction behind the bow shock after shock interaction. It is seen that just ahead of the shoulder heat transfer rates as high as 600 BTU/ft$^2$sec and twice the stagnation point heat transfer are achieved.

A small effect of increasing roughness is seen. This amounts to an earlier decrease in heat transfer rate and a later increase in heat transfer rate with increase in surface roughness. A change in conditions from M = 16, Re = $9\times10^6$ /ft to M = 20, Re = $3\times10^2$ per foot causes a decrease in normalized heat transfer rate similar to (and hence for similar reasons) the zero incidence case.

Negative angle of attack cases : Measurements of heat transfer rate on negative angle of attack surfaces compared with those at zero angle of attack again show a less steep variation in heat transfer rate with distance, giving lower heat transfer rates just before the shoulder. This denotes the presence of slightly later flow separation than for the zero angle of attack case.

As for the other angle of attack cases, there is a trend of slightly decreasing heat transfer rates with increasing surface roughness. Also a change in conditions from M = 16, Re = $9\times10^6$ /ft to M = 20, Re = $3\times10^6$ /ft provides a lowering of the non-dimensional heating rate.

### 3.2.3 Time dependent pressure measurements and photography

The pressure measuring system, although making use of fast response PCB piezo-electric transducers, is limited in response by the pneumatic connection from the surface tap to the transducer. Both the volume of transducer and length of connection was kept to a minimum, however, the frequency response was assessed to be no better than 5 kHz. Furthermore, the U.V. recorder galvanometers used had a response of 5 kHz. This is the standard measuring system used in the Longshot tunnel for measuring quasi steady pressures during the 10 msec duration testing time. Use of flush-mounted gauges was impractical because the transducer heads, which had flat surfaces, were not small enough that they could be considred "contoured" with the surface. Furthermore, it would have been impossible to instrument the model with as much spatial resolution as that obtained using taps.

The copper calorimeter heat transducers, also, have a response time no better than 1 msec, and the signal recorded is an integral of the heat transfer sensed in any case such that data reduction to obtain unsteady information would be difficult. Hence, such instrumentation is unsuitable for measuring flow unsteadiness when present.

The observations for flow unsteadiness were hence based on the pressure measurement signals backed up by ciné photograph sequences at 6000 frames/sec. Examples of photographs taken during an unstable period are shown in figure 8. One channel of pressure measurement near the shoulder was normally recorded on an oscilloscope. However, although the basic frequency of the unsteadiness of approximately 2 kHz was lower than the frequency response of the

system, the signals were characterized by spikes which were not faithfully followed by the signal. This information should be taken into account in the following interpretation.

The region in which the pressure transducers most easily detected flow instability was in the region just ahead of the shoulder. It is in this region that the instantaneous gradient in pressure is the largest, due to the interaction region downstream of the shock wave intersection and hence movement of the shock waves caused by the instability will have most effect. Since the region of very high instantaneous pressure is very localized, then the signal expected will consist of the "spikes" in signal contained in a relatively low pressure level as in fact recorded and alluded to in the last paragraph. This is indeed the case as shown in figure 9.

In nearly all of the cases tested was there found to be stable flow throughout most of the running time of the tests. The experience is found that there are periods during which instability occurs. This would tend to indicate that the shape for the particular conditions tested is intermediate to one being stable and one being unstable. Experience (Ref. 11) has indicated that the boundary between stable and unstable flow is a very sharp one as found by decreasing, in small steps, the length of a spike mounted on a blunt body. In the present tests, a small change in test conditions or a small test flow perturbation could be envisaged to change the flow from a steady to an unsteady flow situation and back again. In the several occasions that repeat tests were made, it was found that instability did not occur at exactly the same period in each test, hence it is concluded that the instability is more likely to be triggered by tunnel flow instabilities rather than gradually changing flow conditions. From neither the ciné schlieren photograph sequences nor the pressure fluctuation photographs was it easy to assess accurately the periods of instability (although a burst of "noise" seen on the pressure traces in the appropriate region was accompanied by changing shock shapes in the photograph at equivalent times) hence in the ensuing discussion,

some subjectivity must be present. Another feature is that signals recorded near reattachment points are likely to be noisy in any case because of the inherent unsteadiness involved with even so called steady flow situations (see Ref. 12).

### 3.2.4 Detailed examination of unsteady flow characteristics

$M_{nom}$ = 16, Re = $9\times10^6$ per foot cases, $\alpha$ = 0° and 3°

At zero angle of attack, mild instability occurs at several times during a test with a larger proportion of time unstable for the smooth model than the rougher model. The frequency is around 2000±10% equivalent to a Strouhal number (Str) of 0.17±10%. This is the same value as found in the previous preliminary study recorded in reference 5.

For the smooth model at 3° angle of attack, the "windward" surface is always found to be unstable, as is the "leeward" surface except for the first two milliseconds. The instability of the leeward surface appears to be forced by the behaviour on the windward surface. The instability of the flow on the windward surface of the model at 3° angle of attack compared to zero angle of attack is expected, because of the shape change presented to the flow : the latter stages of the forebody has a high angle to the flow, and also the change in incidence causes an effective decrease in the "spike length to diameter ratio". Again the frequency of oscillation, very much more evident from the windward pressure tap than the leeward one, indicates a frequency of approximately 2000 (Str = 0.17). With a rougher surface, however, the flow becomes relatively stable as seen on the pressure traces.

$M_{nom}$ = 20, Re = $3\times10^6$ per foot cases, $\alpha$ = 0° and 3°

For the smoother model at zero angle of attack a mild instability is sensed during the whole tets. The frequency is assessed to be around 2100 Hz±10% giving a Strouhal number of approximately 0.16. For the rougher body case, the flow is more stable, but several bursts of instability occur during the test.

The bursts exist for such a small period that it is difficult to assess the frequency of oscillation.

For angle of attack cases mild oscillation is found for all cases. The schlieren photographs recorded at these test conditions are difficult to interpret because of the existence of intense radiation emitted by dust particles heated to high temperatures behind strong (normal) shock waves, which cannot be eliminated.

$M_{nom}$ = 16, Re = $5\times10^6$ per foot cases, $\alpha = 0°$

For both models MR1 and MR2 the flow starts stable and after a certain delay, the flow goes unstable. However, the delay for the model MR2 is longer than for MR2. The frequency is again close to 2000 Hz giving a Strouhal number of 0.16.

$M_{nom}$ = 20, Re = $2\times10^6$ per foot cases, $\alpha = 0°$

For both models, the flow appears quite stable except for bursts of mild instability. The rougher model MR2 shows less instability than the smoother model MR1. The bursts of instability are so short that it is difficult to assess their frequency.

Summarizing, the test series indicate that instabilities occur during part of all the tests. Increased roughness has the effect of suppressing the instabilities. In most of the cases, the instability is amplified when the model incidence is changed to 3° from zero degrees. There appears to be no understandable trend of presence of instability over the range $16 < M < 20$ and $2\times10^6 < Re/ft < 9\times10^6$. The reduced frequency (Strouhal number) of the main instability is approximately 0.16-0.17 over this range of conditions. This agrees with the findings from an earlier, but less complete study carried out in Longshot tunnel and reported in reference 5.

### 3.3 Discussion of results related to evolution of ablation nosetip shapes

The results from this study and earlier studies can be related to the evolution of ablating nose-tips (Fig. 1). Due to transitional flow, then hollow models can be formed by reason of the peak heating occurring away from the stagnation point. For moderately concave models, the interaction obtained causes heat rates to be highest in the concave regions themselves causing the concavity to increase (Ref. 3). At some stage, the concavity reaches such a level, that the flow becomes separated causing the heating peak to shift to the shoulder (Ref. 3). In some cases instabilities occur such as found in the present study. The measurements show several mechanisms for the shoulder to be eroded. Firstly, the heating rate, even the averaged value during unsteady flow situations is highest near the shoulder. Secondly, intense fluctuating loadings on the shoulder caused by the instability could cause a mechanical erosion of the surface. Both of these actions could cause the nosetip to assume the "sharp turbulent" configuration shown in figure 1.

## 4. CONCLUSIONS

Pressure and heat transfer measurements and high speed schlieren visualization of the flow were made on a concave conic shape with a spherical nosetip tested in the flow of the von Karman Institute Longshot facility at nominal Mach numbers of 16 and 20 and Reynolds numbers of $9\times10^6$ and $4.5\times10^6$, and $3.0\times10^6$ and $2.0\times10^6$ per ft respectively. The effect of surface roughness and flow incidence of $\pm3°$ on the measurements was studied. The shape was characterized by being strongly concave (i.e., small longitudinal radius of curvature) with the late stages of the surface showing an angle of 85° to the flow.

For these models and under the test conditions chosen it is found that instabilities having a reduced frequency of approximately 0.17 occur during part of the testing time. Increased surface roughness has the effect of suppressing the instabilities, but the instability is enhanced when the incidence is changed from 0° to 3°. No clear trend of the existence of instability with changing flow conditions occurs.

The time-averaged measurements give heat transfer and pressure distributions typical of those expected of regions of large transitional separation, i.e., flat distributions followed by peaky values near reattachment points occurring just upstream of the reattachment point. The changes in distribution sensed are affected mainly by the flow conditions (changes shear layer transition point) and angle of incidence (changes reattachment point). Surface roughness appears to affect little the measurements within these large separated regions. The high values of heating sensed near the shoulder is likely to cause an ablating nose to achieve a less strongly concave shape.

REFERENCES

1. RICHARDS, B.E. & ENKENHUS, K.R.: Hypersonic testing in the VKI Longshot piston tunnel.
AIAA J., Vol. 8, No 6, June 1970, pp 1020-1025.

2. RICHARDS, B.E.; DiCRISTINA, V.;; MINGES, M.L.: Heat transfer and pressure distribution on sharp and finite bluntness biconic and hemispherical geometries at various angles of attack in a Mach 15-20 flow.
Astronautical Research 1971; ed. L.G. Napolitano;
D. Reidel Publ. Co., Dordrecht, Holland, 1973, pp 91-103.

3. DiCRISTINA, V. & RICHARDS, B.E.: Heat transfer studies on ablation protected nosetips at reentry simulated conditions.
AIAA P 77-781; 12th Thermophysics Conf. Albuquerque, New Mexico, June 1977.

4. RICHARDS, B.E.: Experimental study of the hypersonic flow over a convex conic model resembling the nosetip of a reentry vehicle.
VKI IN 59, Scientific Report for USAF Grant AFOSR 76-2942, February 1978.

5. KENWORTHY, M.A. & RICHARDS, B.E.: A study of the unsteady flow over concave conic model at Mach 15 and 20.
AFML TR 75-138, September 1975.

6. KABELITZ, H.P.: Zur Stabilität geschlossener Grenzschichtablösegebiete an konischen Drehkörper bei Hyperschallströmung.
DLR FB 77-71, 1971.

7. KENWORTHY, M.A.; PANARAS, A.G.; RICHARDS, B.E.; WENDT, J.F.: On unsteady flows generated by shock/shock interactions.
in Shock Tube and Shock Wave Research, Proceedings of the Eleventh International Symposium on Shock Tubes and Waves. University of Washington Press, 1977.

8. RICHARDS, B.E.; CULOTTA, S.; SLECHTEN, J.: Heat transfer and pressure distributions on reentry nose shapes in the VKI Longshot hypersonic tunnel.
AFML TR 71-200, June 1971.

9. RICHARDS, B.E.: Developments in heat transfer measurements using transient techniques.
ICIASF' 77 record. Proc. 7th Int. Congress on Instrumentation in Aerospace Simulation Facilities;
Shrivenham, UK; IEEE Publication 77 CH 1251-8 AES;
September 1977, pp 81-88.

10. BACKX, E. & RICHARDS, B.E.: Measurement of stagnation temperatures of 2500 K in a hypersonic flow of 10 msec duration using a fine wire probe.
ICIASF' 77 Record. Proc. 7th Int. Congress on Instrumentation in Aerospace Simulation Facilities; Shrivenham, UK; IEEE Publication 77 CH 1251-8 AES, September 1977, pp 95-100.

11. KENWORTHY, M.A. & LOLL, V.: Shock instabilities with spiked blunt bodies.
Paper 74-07, Fourth IAF Int. Student Conference, Amsterdam, October 1974;
also VKI Preprint 74-02.

12. HANKEY, W.L. & HOLDEN, M.S.: Two dimensional shock wave/boundary layer interactions.
AGARDograph 203, 1975.

TABLE 1 - HEAT SENSOR CALIBRATION INFORMATION

| Position | Gauge No | Calibration constant used $\frac{B.Th.U/ft^2 sec}{mv / sec}$ |
|---|---|---|
| Stagn.point | 7 | 0.480 |
| A | 20 | 0.676 |
| B | 15 | 0.612 |
| C | 19 | 0.505 |
| D | 14 | 0.606 |
| E | 5 | 0.654 |
| F | 2 | 0.671 |
| G | 18 | 0.585 |
| H | 16 | 0.625 |
| I | 6 | 0.548 |
| J | 17 | 0.595 |

TABLE 2 - TEST IDENTIFICATION

| INCIDENCE | 0° | | +3° ⁂ | | -3° | |
|---|---|---|---|---|---|---|
| MODEL | MR1 | MR2 | MR1 | MR2 | MR1 | MR2 |
| M = 16<br>Re = $9\times10^6$ | 586<br>(596) | 600<br>(599) | 594<br>(595) | 607 | 593 | 606 |
| M = 16<br>Re = $5\times10^6$ | 588<br>(598) | 601 | - | - | - | - |
| M = 20<br>Re = $3\times10^6$ | 589 | 603 | 591 | 604 | 592 | 605 |
| M = 20<br>Re = $2\times10^6$ | 590 | 602 | - | - | - | - |

⁂
- positive incidence means top surface is leeward
- top surface is the one with the first measuring station after the stagnation point fitted with a pressure tap
- in the graphs +ve incidence means a windward surface

TABLE 3 - TEST MATRIX AND CONDITIONS

| RUN | MODEL | INCID. (deg.) | $P_0$ (lb/in$^2$) | $P_{0perf}$ (lb/in$^2$) | $T_0$ (K) | $T_{0perf}$ (K) | $T_{stag}$ (K) | $Pt_2$ (lb/in$^2$) | M | Re $10^{-6}$ ($ft^{-1}$) | $p \times 10^2$ (lb/in$^2$) | T (K) | $T_{cond}$ (K) | V (ft/sec) | $Q^{\dagger}$ ($\frac{BThU}{ft^2 sec}$) |
|---|---|---|---|---|---|---|---|---|---|---|---|---|---|---|---|
| 586 | MR1 | 0 | 51200 | 72000 | 1890 | 2420 | 2160 | 27.85 | 15.4 | 8.9 | 9.0 | 50 | 43 | 7280 | 270 |
| 588 | | 0 | 38100 | 44100 | 2030 | 2500 | 2230 | 13.3 | 16.2 | 4.5 | 3.9 | 47 | 40 | 7410 | 194 |
| 589 | | 0 | 54900 | 63300 | 2400 | 3070 | 2690 | 7.8 | 19.5 | 2.9 | 1.6 | 40 | 36 | 8230 | 190 |
| 590 | | 0 | 41000 | 39200 | 2610 | 3250 | 2830 | 6.0 | 18.7 | 1.8 | 1.3 | 46 | 35 | 8470 | 177 |
| 591 | | +3 | 54600 | 63100 | 2390 | 3050 | 2670 | 7.8 | 19.5 | 2.9 | 1.6 | 40 | 36 | 8210 | 188 |
| 592 | | -3 | 55100 | 62800 | 2430 | 3110 | 2720 | 7.6 | 19.6 | 2.8 | 1.5 | 40 | 36 | 8290 | 190 |
| 593 | | -3 | 50300 | 71300 | 1860 | 2370 | 2120 | 27.9 | 15.4 | 9.1 | 9.0 | 49 | 44 | 7210 | 264 |
| 594 | | +3 | 49800 | 69800 | 1870 | 2380 | 2130 | 29.2 | 15.2 | 9.2 | 9.7 | 51 | 44 | 7230 | 272 |
| 600 | MR2 | 0 | 50200 | 72500 | 1820 | 2320 | 2090 | 31.5 | 15.1 | 10.1 | 10.6 | 50 | 44 | 7130 | 274 |
| 601 | | 0 | 37600 | 43500 | 2020 | 2490 | 2220 | 18.3 | 15.2 | 5.3 | 6.1 | 53 | 42 | 7380 | 202 |
| 602 | | 0 | 38900 | 38700 | 2450 | 3030 | 2660 | 4.8 | 19.5 | 1.8 | 0.97 | 40 | 34 | 8100 | 147 |
| 603 | | 0 | 51900 | 58300 | 2400 | 3060 | 2680 | 7.2 | 19.5 | 2.7 | 1.5 | 40 | 36 | 8210 | 172 |
| 604 | | +3 | 53400 | 60300 | 2420 | 3080 | 2700 | 8.3 | 19.1 | 2.9 | 1.8 | 42 | 36 | 8250 | 196 |
| 605 | | -3 | 55100 | 62800 | 2430 | 3110 | 2720 | 7.6 | 19.6 | 2.8 | 1.5 | 40 | 36 | 8290 | 190 |
| 606 | | -3 | 48000 | 66300 | 1860 | 2360 | 2120 | 29.7 | 15.0 | 9.2 | 10.2 | 52 | 44 | 7190 | 272 |
| 607 | | +3 | 53200 | 78100 | 1850 | 2380 | 2130 | 30.6 | 15.4 | 9.9 | 9.9 | 49 | 44 | 7220 | 278 |

$^{\dagger}$ theoretical stagnation point heat transfer on 0.437 in radius hemisphere

TABLE 4 - HEAT TRANSFER MEASUREMENTS

| M | Re $10^{-6}$ $ft^{-1}$ | MODEL | INCID. degrees | RUN No. | STAG. PT | HT1 A $b^{\dagger}$ | HT6 B t | HT2 C b | HT7 D t | HT3 E b | HT8 F t | HT4 G b | HT10 H s | HT9 I t | HT5 J b |
|---|---|---|---|---|---|---|---|---|---|---|---|---|---|---|---|
| 15.4 | 8.9 | MR1 | 0 | 586 | 243 | 51 | 66 | 51 | 90 | 60 | 108 | 117 | 85 | 225 | 391 |
| 15.2 | 9.2 | | +3 | 594 | 244 | 70 | 68 | 93 | 79 | 126 | 82 | 197 | 243 | 132 | 499 |
| 15.4 | 9.1 | | -3 | 593 | 342 | 63 | 110 | 61 | 235 | 89 | 274 | 93 | 124 | 397 | 207 |
| 15.1 | 10.1 | MR2 | 0 | 600 | 223 | 33 | 47 | 43 | 55 | 39 | 37 | 100 | 168 | 240 | 361 |
| 15.4 | 9.9 | | +3 | 607 | 255 | 70 | 56 | 82 | - | 69 | - | 198 | 344 | 107 | 566 |
| 15.0 | 9.2 | | -3 | 606 | 253 | 57 | 73 | 50 | 97 | 39 | 167 | 42 | 75 | 515 | 147 |
| 16.2 | 4.5 | MR1 | 0 | 588 | 215 | 40 | 57 | 53 | 77 | 78 | 119 | 140 | 160 | 231 | 358 |
| 15.2 | 5.3 | MR2 | 0 | 601 | 266 | 27 | 36 | 31 | 46 | 30 | 74 | 75 | 118 | 200 | 307 |
| 19.5 | 2.9 | MR1 | 0 | 589 | 156 | 29 | 31 | 39 | 49 | 33 | 54 | - | 86 | 129 | 209 |
| 19.5 | 2.9 | | +3 | 591 | 176 | 43 | 46 | 75 | 50 | 53 | 49 | 135 | 172 | 66 | 260 |
| 19.6 | 2.8 | | -3 | 592 | 203 | 49 | 50 | 42 | 101 | 46 | 165 | 64 | 76 | 202 | 105 |
| 19.5 | 2.7 | MR2 | 0 | 603 | 167 | 30 | 19 | 32 | 29 | 29 | 48 | 57 | 108 | 145 | 216 |
| 19.1 | 2.9 | | +3 | 604 | 190 | 46 | 28 | 49 | 32 | 57 | 37 | 152 | 234 | 75 | 244 |
| 19.6 | 2.8 | | -3 | 605 | 193 | 35 | 39 | 35 | 66 | 24 | 107 | 43 | 76 | 262 | 99 |
| 18.7 | 1.8 | MR1 | 0 | 590 | 138 | 16 | 20 | 24 | 32 | 23 | 35 | 52 | 54 | 104 | 179 |
| 19.5 | 1.8 | MR2 | 0 | 602 | 108 | 12 | 16 | 16 | 20 | 20 | 27 | 35 | 58 | 107 | 184 |

$^{\dagger}$ code : b - gauge on bottom of model; t - top; s - side
+ ve incidence means top surface is leeward

TABLE 5 - NON-DIMENSIONALIZED* HEAT TRANSFER MEASUREMENTS

| M | Re $10^{-6}$ $ft^{-1}$ | MODEL | INCID. degrees | RUN No | THEOR STAG. PT | STAG. PT | A b | B t | C b | D t | E b | F t | G b | H s | I t | J b |
|---|---|---|---|---|---|---|---|---|---|---|---|---|---|---|---|---|
| 15.4 | 8.9 | MR1 | 0 | 586 | 270 | 0.90 | 0.189 | 0.244 | 0.189 | 0.333 | 0.222 | 0.400 | 0.433 | 0.315 | 0.833 | 1.448 |
| 15.2 | 9.2 | | +3 | 594 | 272 | 0.897 | 0.257 | 0.250 | 0.342 | 0.290 | 0.463 | 0.301 | 0.724 | 0.893 | 0.485 | 1.83 |
| 15.4 | 9.1 | | -3 | 593 | 264 | 1.295 | 0.239 | 0.417 | 0.231 | 0.890 | 0.337 | 1.038 | 0.352 | 0.470 | 1.504 | 0.784 |
| 15.1 | 10.1 | MR2 | 0 | 600 | 274 | 0.814 | 0.120 | 0.172 | 0.157 | 0.201 | 0.142 | 0.135 | 0.365 | 0.613 | 0.876 | 1.318 |
| 15.4 | 9.9 | | +3 | 607 | 278 | 0.917 | 0.252 | 0.201 | 0.295 | - | 0.248 | - | 0.712 | 1.237 | 0.385 | 2.036 |
| 15.0 | 9.2 | | -3 | 606 | 272 | 0.930 | 0.210 | 0.268 | 0.184 | 0.357 | 0.143 | 0.614 | 0.154 | 0.276 | 1.893 | 0.540 |
| 16.2 | 4.5 | MR1 | 0 | 588 | 194 | 1.108 | 0.206 | 0.294 | 0.273 | 0.397 | 0.402 | 0.613 | 0.722 | 0.825 | 1.191 | 1.845 |
| 15.2 | 5.3 | MR2 | 0 | 601 | 202 | 1.177 | 0.119 | 0.159 | 0.137 | 0.204 | 0.133 | 0.327 | 0.332 | 0.522 | 0.885 | 1.358 |
| 19.5 | 2.9 | MR1 | 0 | 589 | 190 | 0.821 | 0.153 | 0.163 | 0.205 | 0.253 | 0.174 | 0.284 | - | 0.453 | 0.679 | 1.10 |
| 19.5 | 2.9 | | +3 | 591 | 188 | 0.936 | 0.229 | 0.245 | 0.399 | 0.266 | 0.282 | 0.261 | 0.718 | 0.915 | 0.351 | 1.383 |
| 19.6 | 2.8 | | -3 | 592 | 190 | 1.068 | 0.258 | 0.263 | 0.221 | 0.532 | 0.242 | 0.868 | 0.337 | 0.400 | 1.063 | 0.553 |
| 19.5 | 2.7 | MR2 | 0 | 603 | 172 | 0.923 | 0.166 | 0.105 | 0.177 | 0.160 | 0.160 | 0.265 | 0.315 | 0.597 | 0.801 | 0.840 |
| 19.1 | 2.9 | | +3 | 604 | 196 | 0.969 | 0.235 | 0.143 | 0.250 | 0.163 | 0.291 | 0.189 | 0.776 | 1.194 | 0.383 | 1.245 |
| 19.6 | 2.8 | | -3 | 605 | 190 | 1.016 | 0.184 | 0.205 | 0.184 | 0.347 | 0.126 | 0.563 | 0.226 | 0.400 | 1.380 | 0.521 |
| 18.7 | 1.8 | MR1 | 0 | 590 | 177 | 0.780 | 0.090 | 0.113 | 0.136 | 0.181 | 0.130 | 0.198 | 0.294 | 0.305 | 0.588 | 1.011 |
| 19.5 | 1.8 | MR2 | 0 | 602 | 147 | 0.735 | 0.082 | 0.109 | 0.109 | 0.136 | 0.136 | 0.184 | 0.238 | 0.395 | 0.728 | 1.252 |

* with respect to the theoretical stagnation point heat transfer on 0.437 in sphere

TABLE 6 - PRESSURE MEASUREMENTS

| M | Re $10^{-6}$ $ft^{-1}$ | MODEL | INCID. degrees | RUN No. | PITOT | A t † | B b | C t | D b | E t | F b | G t | H t | I b |
|---|---|---|---|---|---|---|---|---|---|---|---|---|---|---|
| 15.4 | 8.9 | MR1 | 0 | 586 | 27.9 | 11.2 | 11.6 | 10.1 | 12.2 | 12.1 | 11.3 | 10.5 | - | - |
| 15.2 | 9.2 | | +3 * | 594 | 29.2 | 9.0 | - | 8.7 | 8.7 | 9.0 | 11.5 | 8.4 | 12.2 | - |
| 15.4 | 9.1 | | -3 | 593 | 27.9 | 10.7 | 9.4 | 9.1 | 9.4 | 9.5 | 12.3 | 13.2 | 19.6 | - |
| 15.1 | 10.1 | MR2 | 0 | 600 | 31.5 | 10.6 | 10.8 | 10.6 | 11.1 | 11.2 | 10.0 | 10.2 | 11.7 | 16.9 |
| 15.4 | 9.9 | | +3 | 607 | 30.6 | 9.8 | 9.9 | 11.2 | 10.6 | 11.0 | 12.0 | 9.9 | 11.6 | 49.0 |
| 15.0 | 9.2 | | -3 | 606 | 29.7 | 11.2 | 11.3 | 11.2 | 11.1 | 11.6 | 11.2 | 14.5 | 21.0 | 28.9 |
| 16.2 | 4.5 | MR1 | 0 | 588 | 18.3 | 7.1 | 7.4 | 8.7 | 6.6 | 7.8 | 7.0 | 7.1 | 9.5 | - |
| 15.2 | 5.3 | MR2 | 0 | 601 | 18.3 | 7.1 | 7.7 | 8.1 | 7.7 | 7.7 | 7.3 | 7.1 | 8.4 | 12.6 |
| 19.5 | 2.9 | MR1 | 0 | 589 | 7.84 | 3.7 | 4.0 | - | 3.4 | 3.8 | 3.3 | 3.2 | 3.9 | - |
| 19.5 | 2.9 | | +3 | 591 | 7.80 | 3.02 | 3.02 | 2.62 | 2.76 | 2.95 | 3.55 | 3.08 | 3.32 | - |
| 19.6 | 2.8 | | -3 | 592 | 7.64 | 3.19 | 4.24 | 2.43 | 2.81 | 3.30 | 3.64 | 3.59 | 5.66 | - |
| 19.5 | 2.7 | MR2 | 0 | 603 | 7.20 | 3.23 | 3.30 | 3.85 | 3.24 | 2.25 | 3.44 | 3.32 | 4.13 | 5.64 |
| 19.1 | 2.9 | | +3 | 604 | 8.29 | 3.03 | 3.02 | 3.38 | 3.47 | 3.54 | 4.52 | 4.13 | 3.76 | 9.46 |
| 19.6 | 2.8 | | -3 | 605 | 7.44 | 3.27 | 3.20 | 3.44 | 3.25 | 4.06 | 3.55 | 5.16 | 6.97 | 3.1 |
| 18.7 | 1.8 | MR1 | 0 | 590 | 5.50 | 2.25 | 2.58 | 2.06 | 2.03 | 2.12 | 2.28 | 2.18 | 2.68 | - |
| 19.5 | 1.8 | MR2 | 0 | 602 | 4.81 | 2.10 | 2.24 | 2.20 | 2.12 | 2.24 | 2.14 | 2.12 | 2.76 | 4.19 |

† code : b - gauge on bottom of model; t - top; s -side

* +ve incidence means top surface is leeward

TABLE 7 - NON-DIMENSIONAL PRESSURE MEASUREMENTS

| M | Re $10^{-6}$ $ft^{-1}$ | MODEL | INCID. degrees | RUN No. | A t | B b | C t | D b | E t | F b | G t | H t | I b |
|---|---|---|---|---|---|---|---|---|---|---|---|---|---|
| 15.4 | 8.9 | MR1 | 0 | 586 | 0.401 | 0.416 | 0.362 | 0.437 | 0.434 | 0.405 | 0.376 | - | - |
| 15.2 | 9.2 | | +3 | 594 | 0.308 | - | 0.298 | 0.298 | 0.308 | 0.394 | 0.288 | 0.418 | - |
| 15.4 | 9.1 | | -3 | 593 | 0.386 | 0.337 | 0.326 | 0.337 | 0.341 | 0.441 | 0.477 | 0.703 | - |
| 15.1 | 10.1 | MR2 | 0 | 600 | 0.337 | 0.343 | 0.337 | 0.352 | 0.356 | 0.317 | 0.324 | 0.371 | 0.536 |
| 15.4 | 9.9 | | +3 | 607 | 0.320 | 0.324 | 0.366 | 0.346 | 0.359 | 0.392 | 0.324 | 0.379 | 1.600 |
| 15.0 | 9.2 | | -3 | 606 | 0.377 | 0.380 | 0.377 | 0.374 | 0.391 | 0.377 | 0.488 | 0.707 | 0.973 |
| 16.2 | 4.5 | MR1 | 0 | 588 | 0.388 | 0.404 | 0.475 | 0.361 | 0.426 | 0.383 | 0.388 | 0.519 | - |
| 15.2 | 5.3 | MR2 | 0 | 601 | 0.388 | 0.421 | 0.443 | 0.421 | 0.421 | 0.399 | 0.388 | 0.459 | 0.689 |
| 19.5 | 2.9 | MR1 | 0 | 589 | 0.472 | 0.510 | - | 0.306 | 0.485 | 0.421 | 0.408 | 0.497 | - |
| 19.5 | 2.9 | | +3 | 591 | 0.387 | 0.387 | 0.336 | 0.354 | 0.378 | 0.455 | 0.395 | 0.426 | - |
| 19.6 | 2.8 | | -3 | 592 | 0.418 | 0.555 | 0.318 | 0.368 | 0.432 | 0.476 | 0.470 | 0.741 | - |
| 19.5 | 2.7 | MR2 | 0 | 603 | 0.449 | 0.458 | 0.535 | 0.450 | 0.313 | 0.478 | 0.461 | 0.574 | 0.783 |
| 19.1 | 2.9 | | +3 | 604 | 0.366 | 0.364 | 0.408 | 0.419 | 0.427 | 0.545 | 0.495 | 0.453 | 1.141 |
| 19.6 | 2.8 | | -3 | 605 | 0.440 | 0.430 | 0.462 | 0.437 | 0.546 | 0.477 | 0.694 | 0.937 | 0.417 |
| 18.7 | 1.8 | MR1 | 0 | 590 | 0.409 | 0.459 | 0.375 | 0.369 | 0.385 | 0.415 | 0.396 | 0.487 | - |
| 19.5 | 1.8 | MR2 | 0 | 602 | 0.437 | 0.466 | 0.457 | 0.441 | 0.466 | 0.445 | 0.441 | 0.555 | 0.871 |

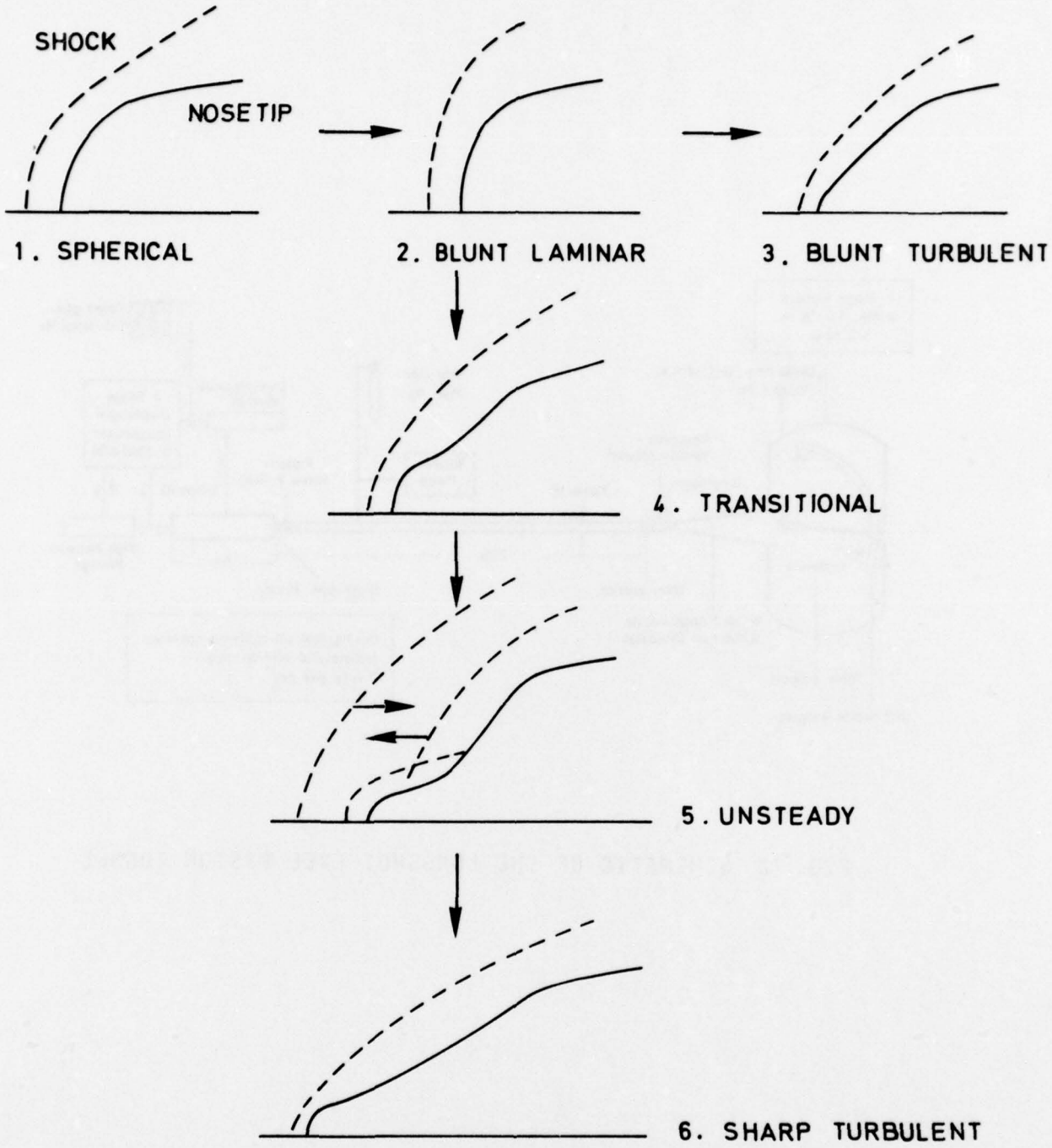


FIG. 1 - NOSETIP SHAPE EVOLUTION

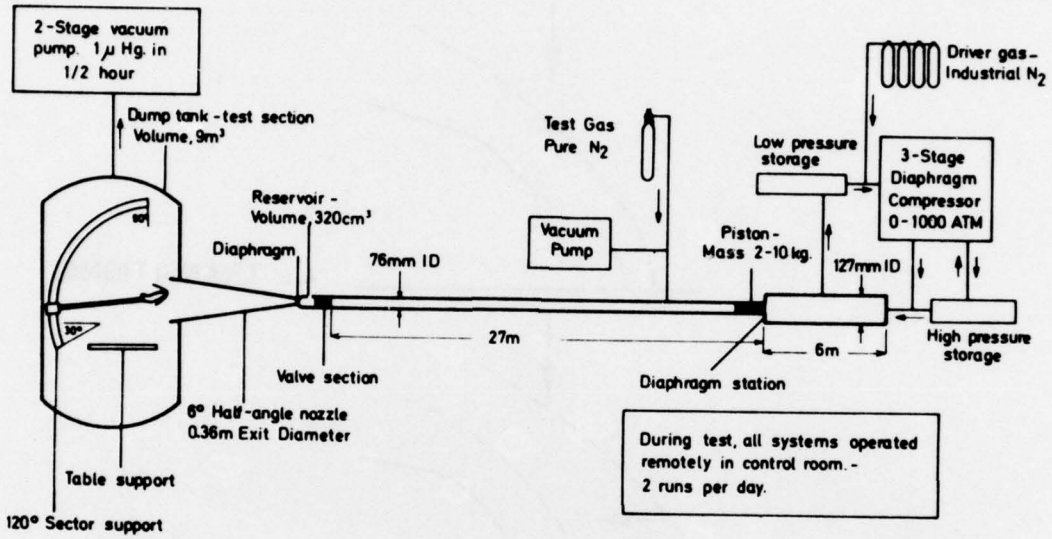


FIG. 2 SCHEMATIC OF THE LONGSHOT FREE PISTON TUNNEL

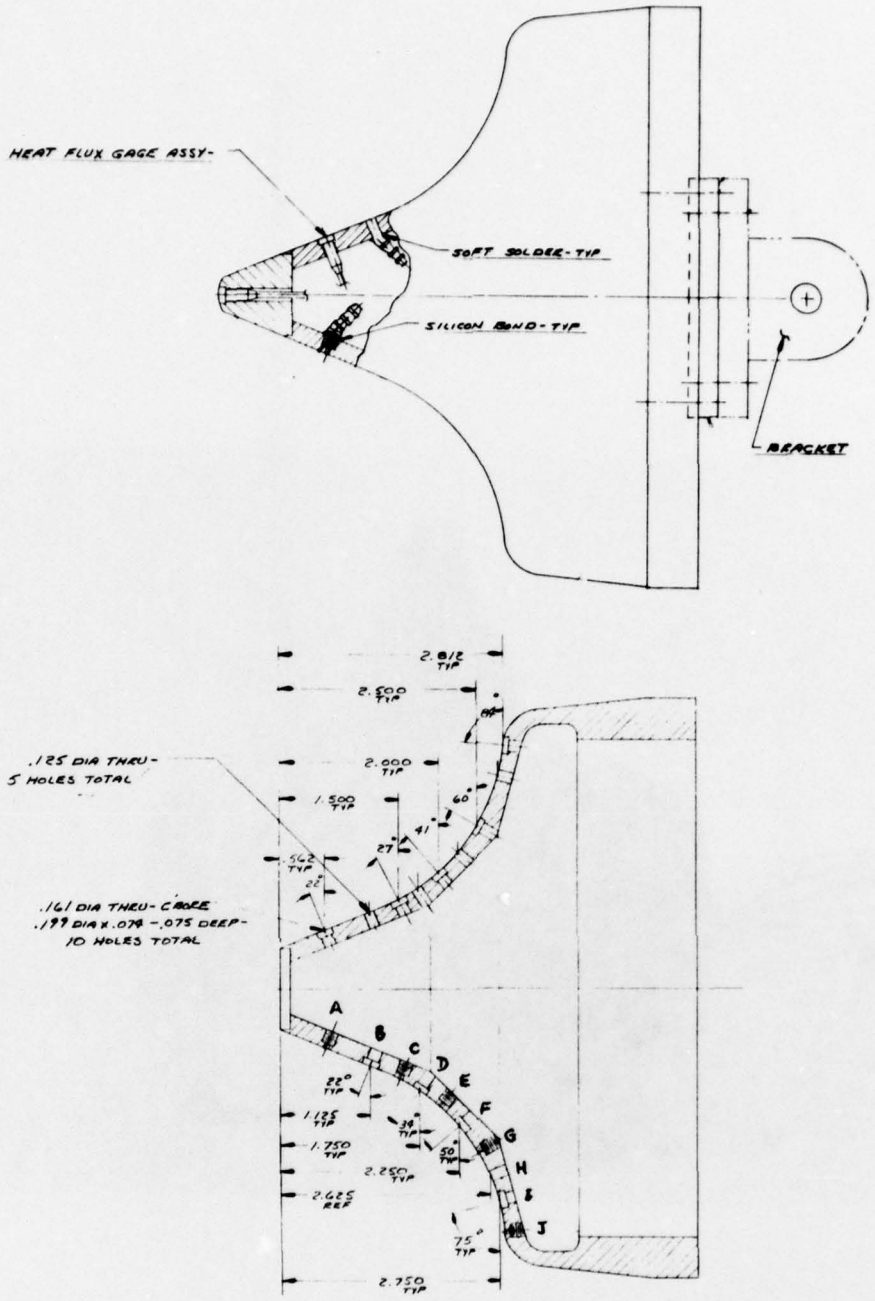


DIMENSIONS IN INCHES

POSITION OF GAUGES, S, INS. FROM STAG. PT

| POS | A | B | C | D | E | F | G | H | I | J |
|---|---|---|---|---|---|---|---|---|---|---|
| S ins | 1.6 | 2.2 | 2.6 | 2.9 | 3.3 | 3.6 | 4.0 | 4.4 | 4.7 | 5.5 |

FIG. 3 - SCHEMATIC OF MODELS MR1, MR2.

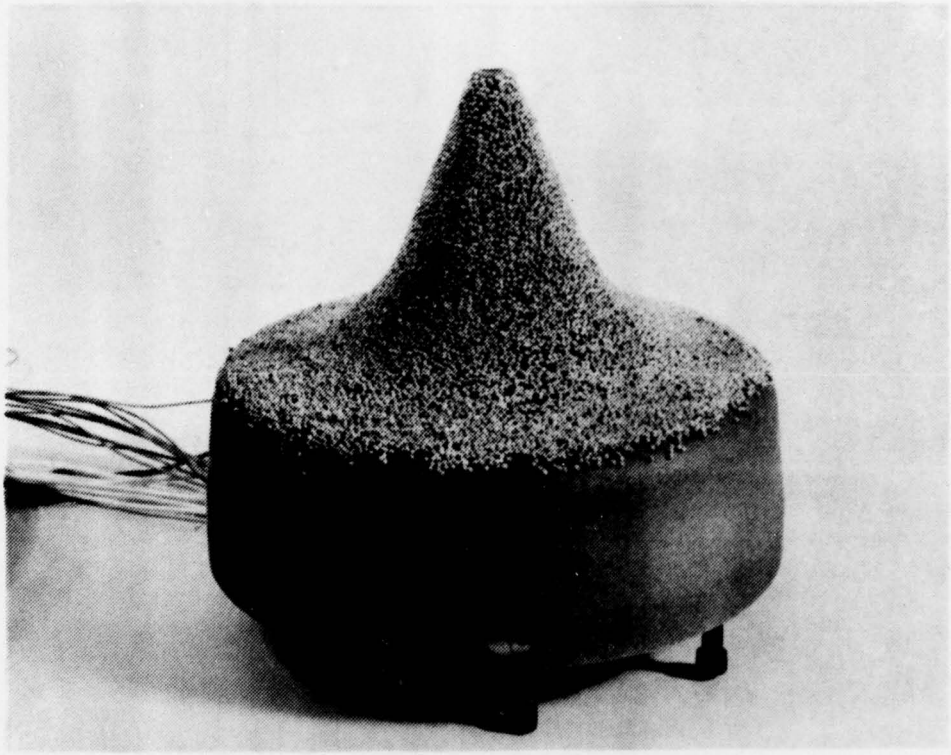

FIG. 4 - PHOTOGRAPH OF MODEL M R 2

MODEL MR1

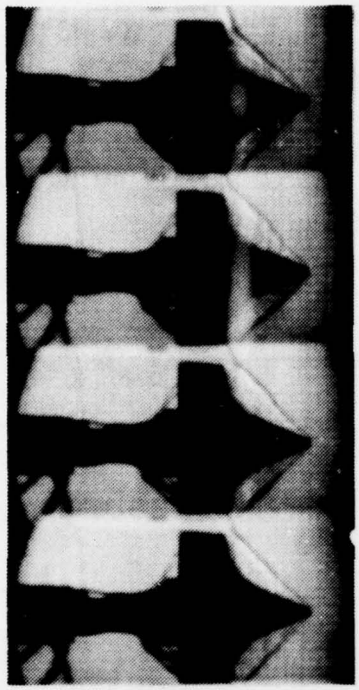

I) RUN 596, $\alpha = 0°$

MODEL MR2

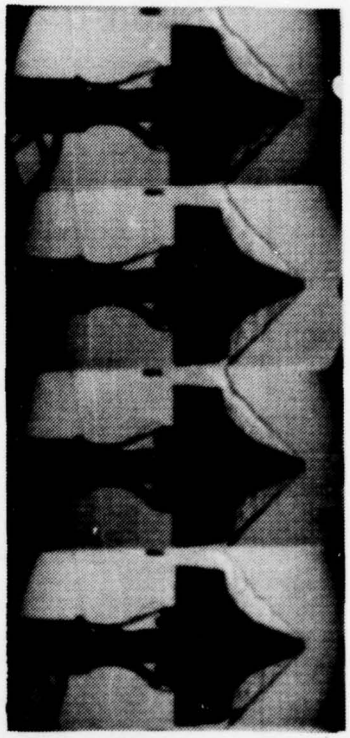

II) RUN 600

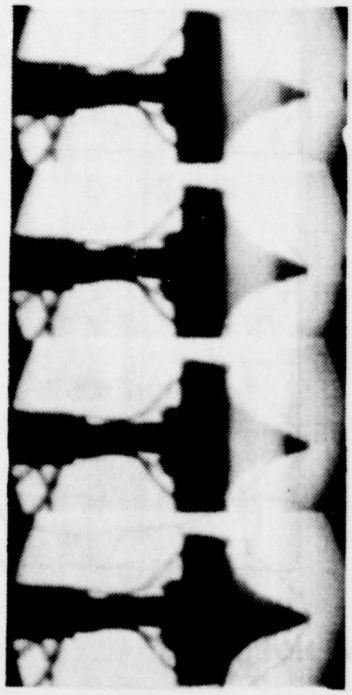

III) RUN 593, $\alpha = 3°$

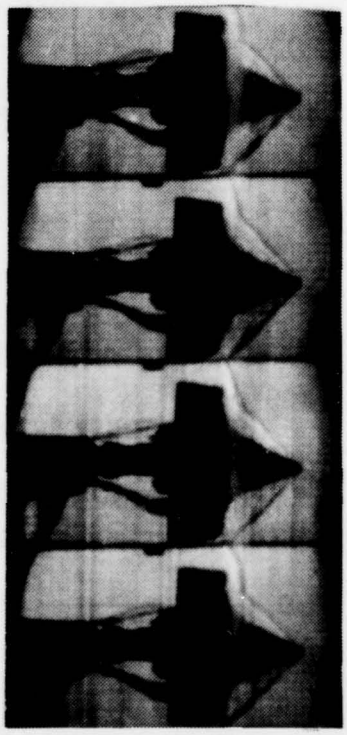

IV) RUN 606, $\alpha = 3°$

FIG. 5 a - SCHLIEREN PHOTOGRAPHS $M = 16$, $R_e = 9 \times 10^6/ft$.

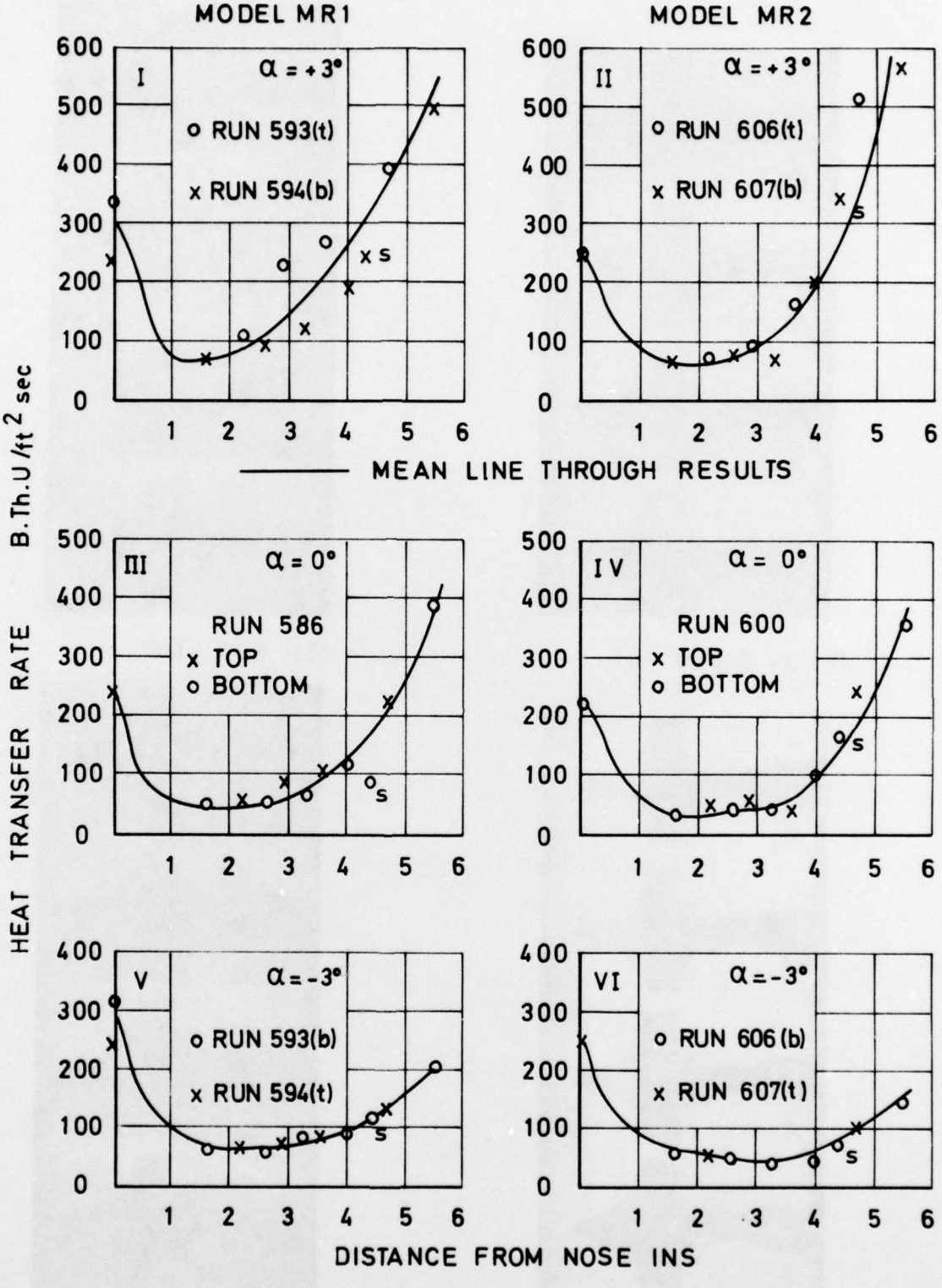


FIG.5b _ HEAT TRANSFER MEASUREMENTS

$M = 16$, $R_e = 9 \times 10^6$/ ft

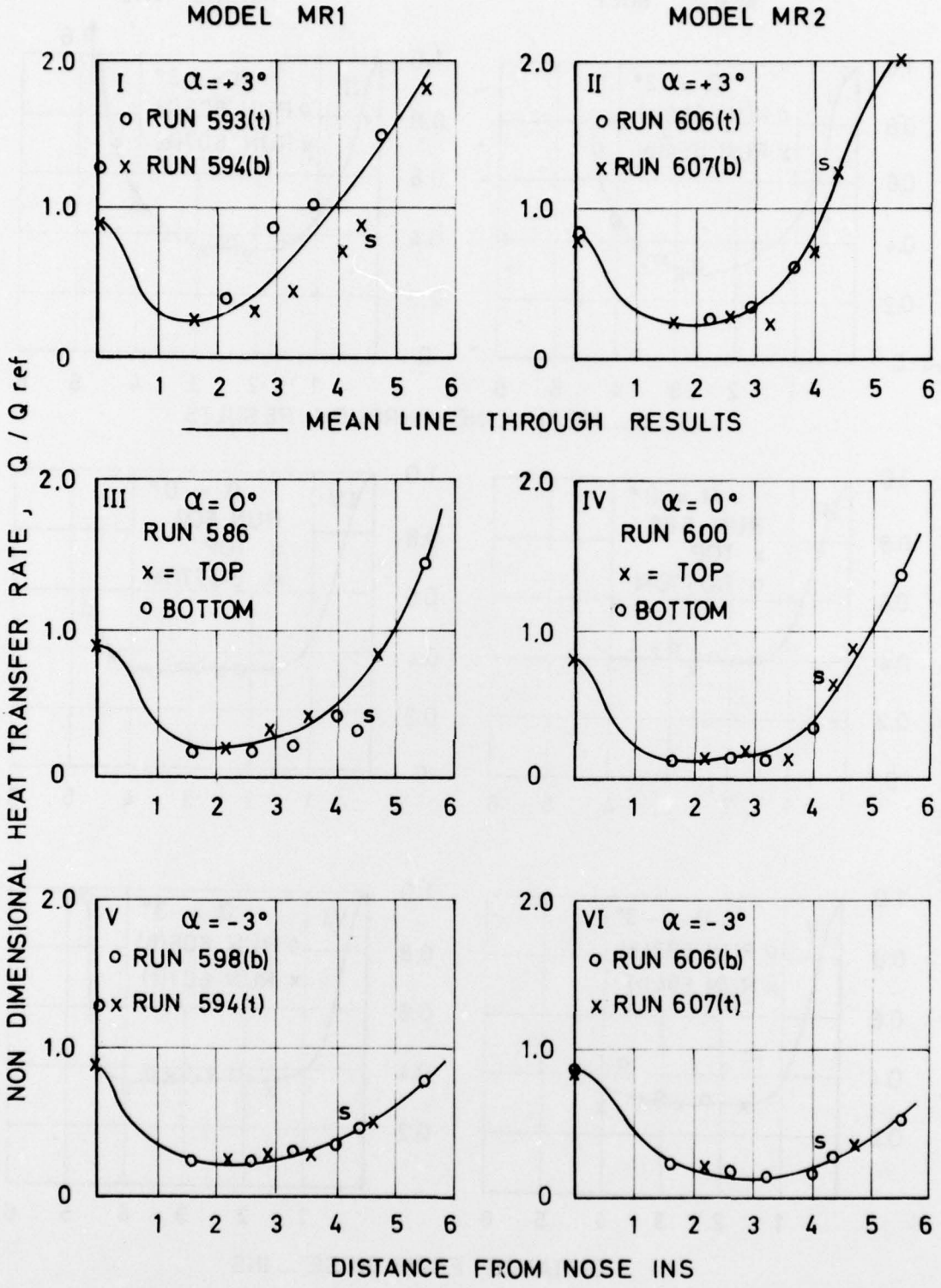


FIG. 5c – NON-DIMENSIONAL HEAT TRANSFER MEASUREMENTS

$M = 16$, $R_e = 9 \times 10^6$/ft

Q REF. IS THEORETICAL STAGNATION POINT HEAT TRANSFER.

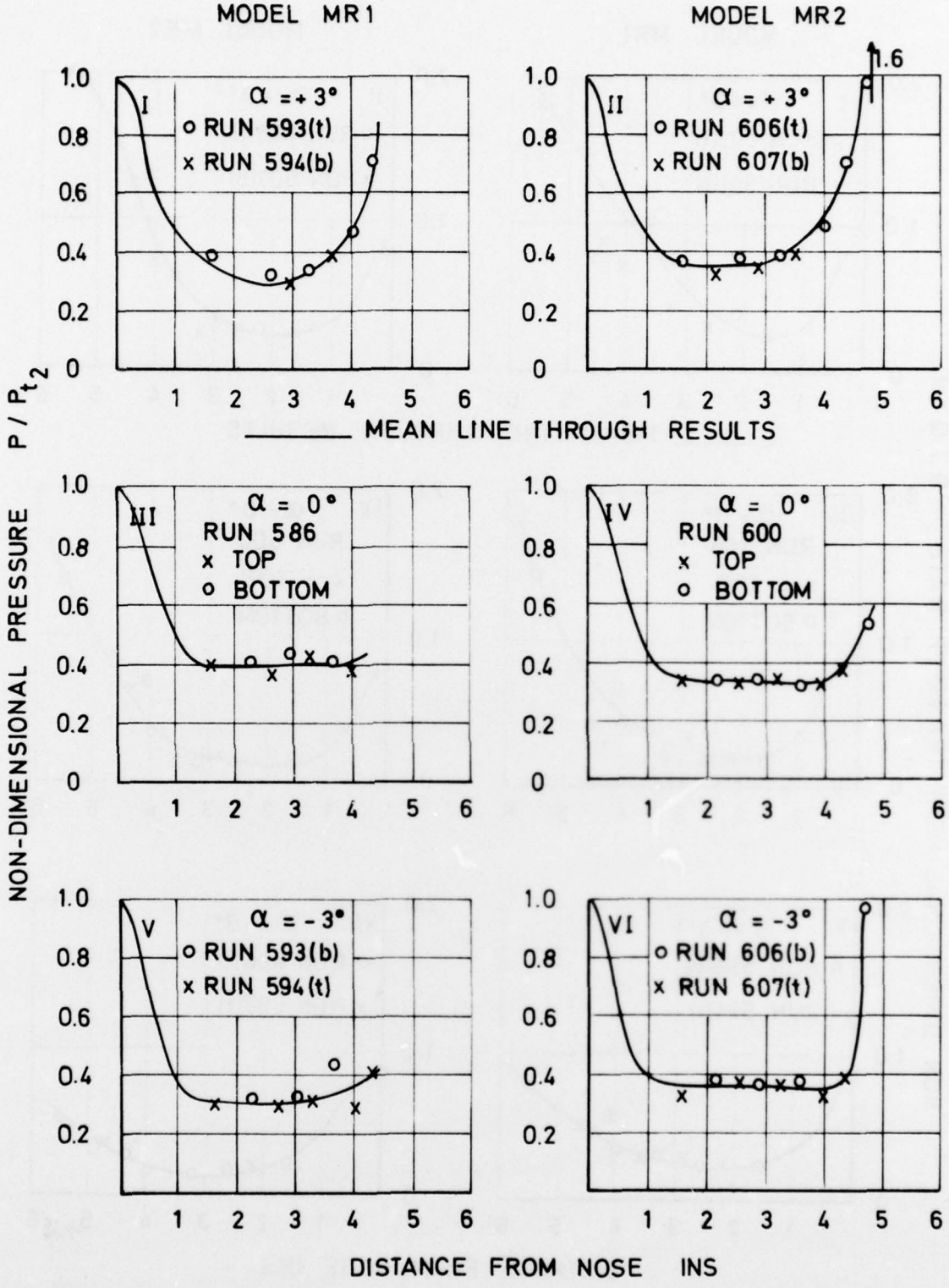


FIG. 5d NON-DIMENSIONAL PRESSURE MEASUREMENTS

$M = 16, \quad R_e = 9 \times 10^6 / ft$

MODEL MR1

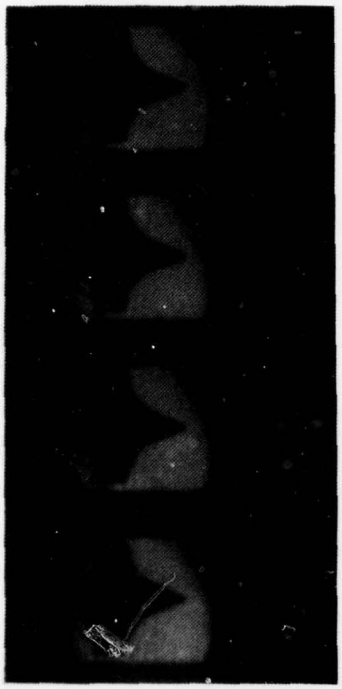

I) RUN 589, $\alpha = 0$

MODEL MR2

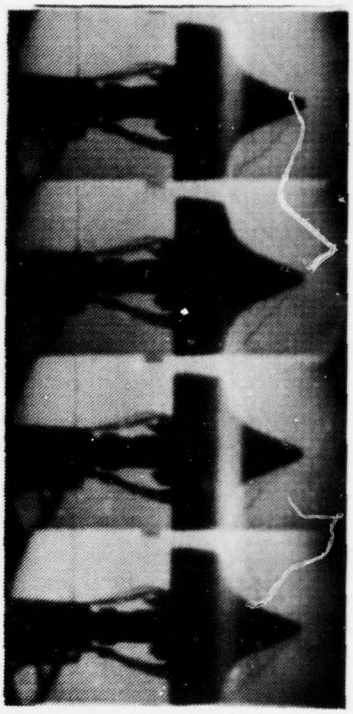

II) RUN 603, $\alpha = 0°$

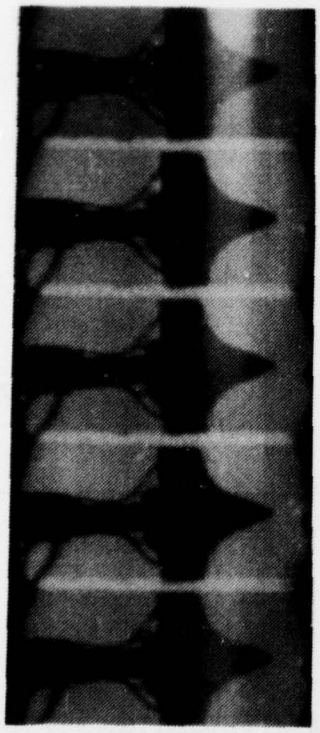

III) RUN 591, $\alpha = 0$

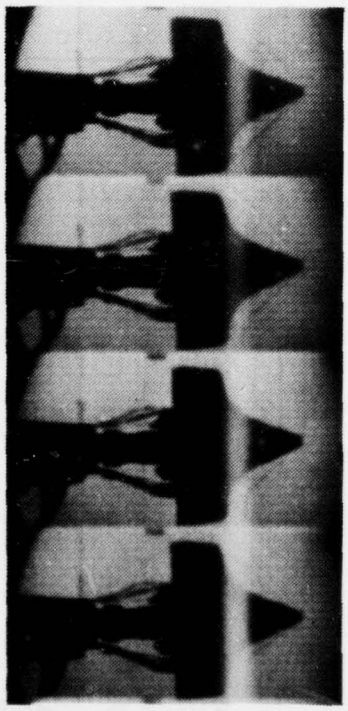

IV) RUN 605, $\alpha = 3°$

FIG. 6 a - SCHLIEREN PHOTOGRAPHS , $M = 20$ , $R_e = 3 \times 10^6 / ft$

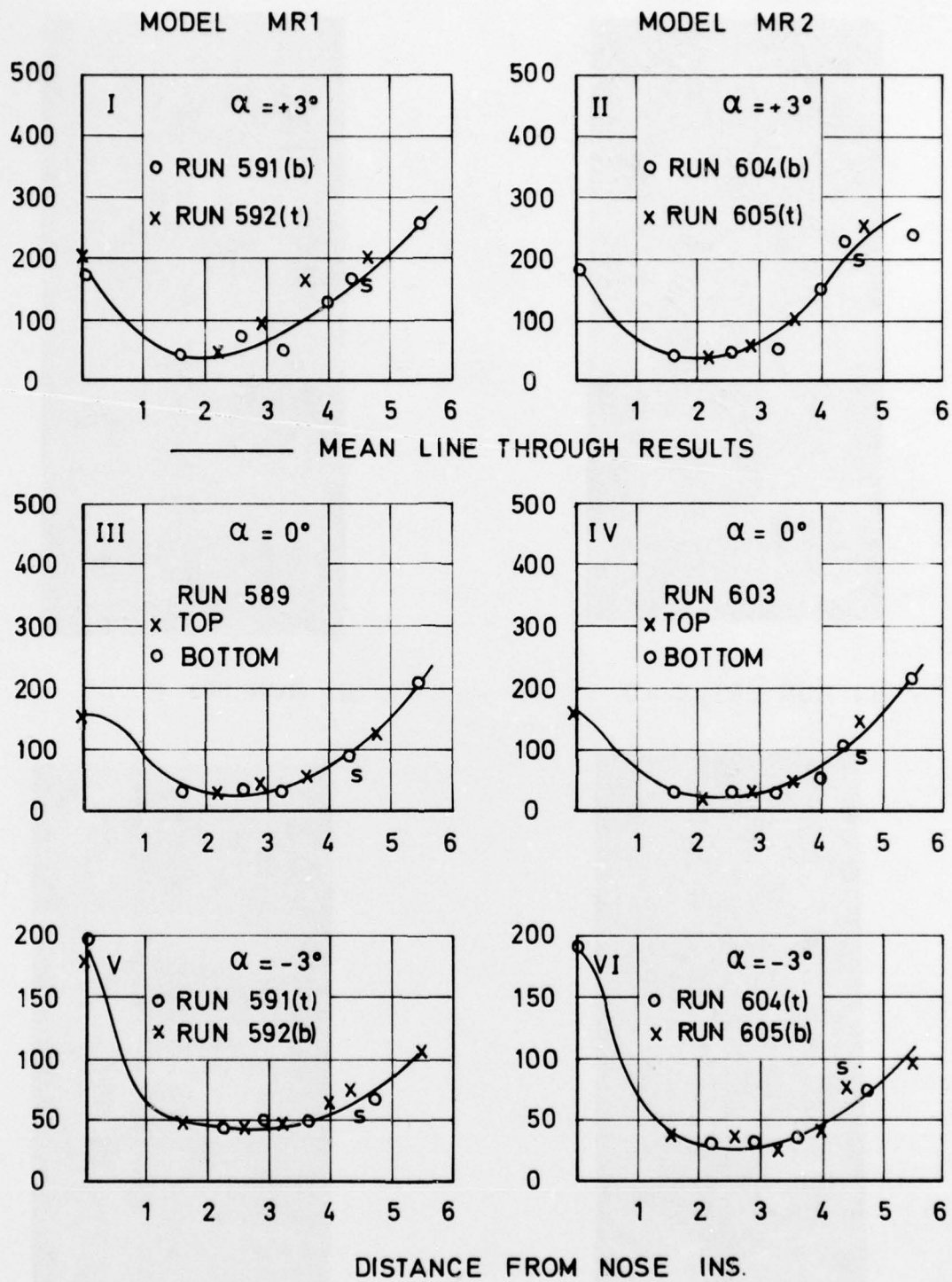


FIG. 6 b _ HEAT TRANSFER MEASUREMENTS

$M = 19$, $R_e = 3 \times 10^6/ft$

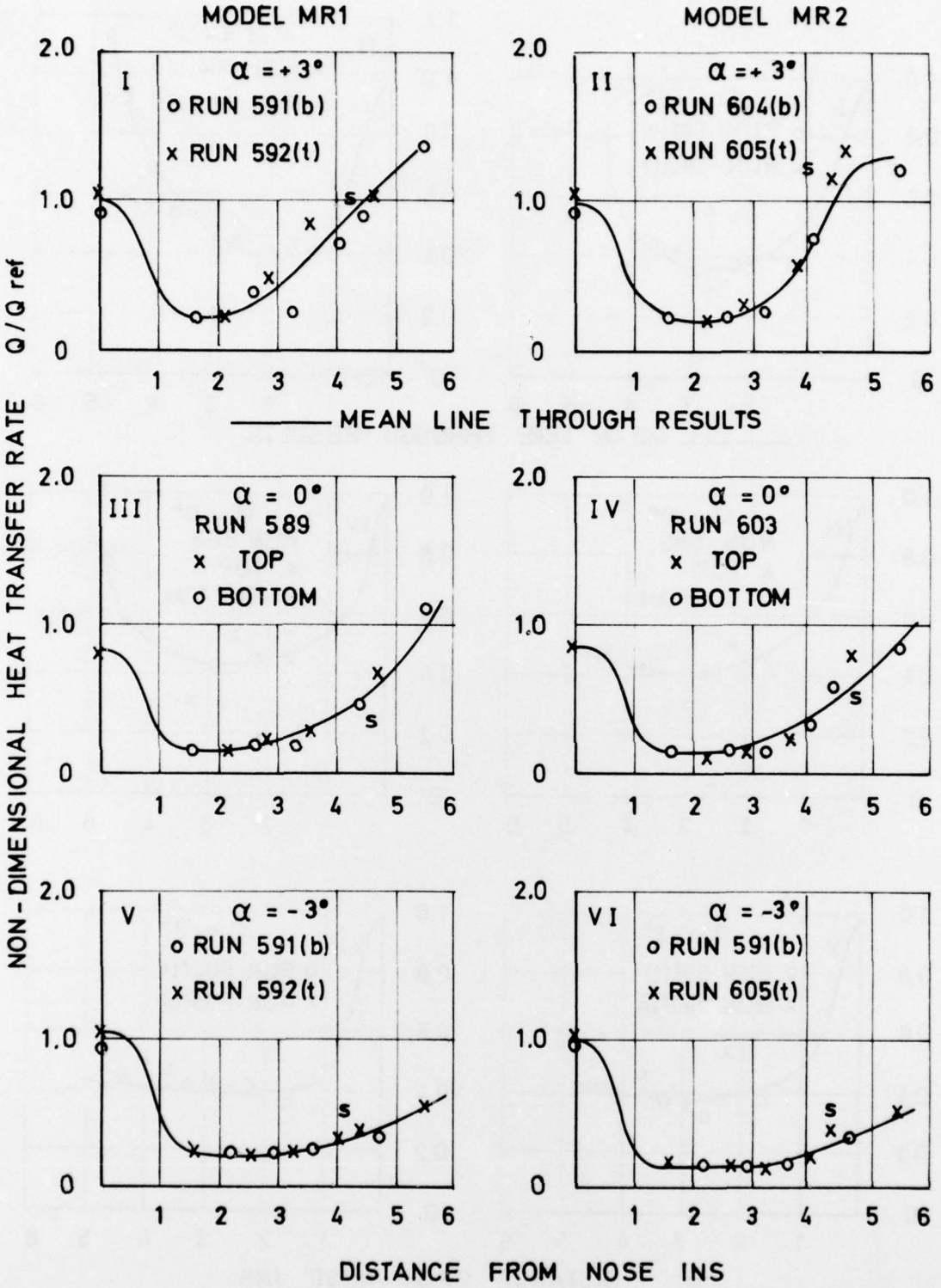


FIG. 6c — NON-DIMENSIONAL HEAT TRANSFER MEASUREMENT
$M = 19$, $R_e = 3 \times 10^6$/ft
Q REF IS THEORETICAL STAGNATION POINT HEAT TRANSFER.

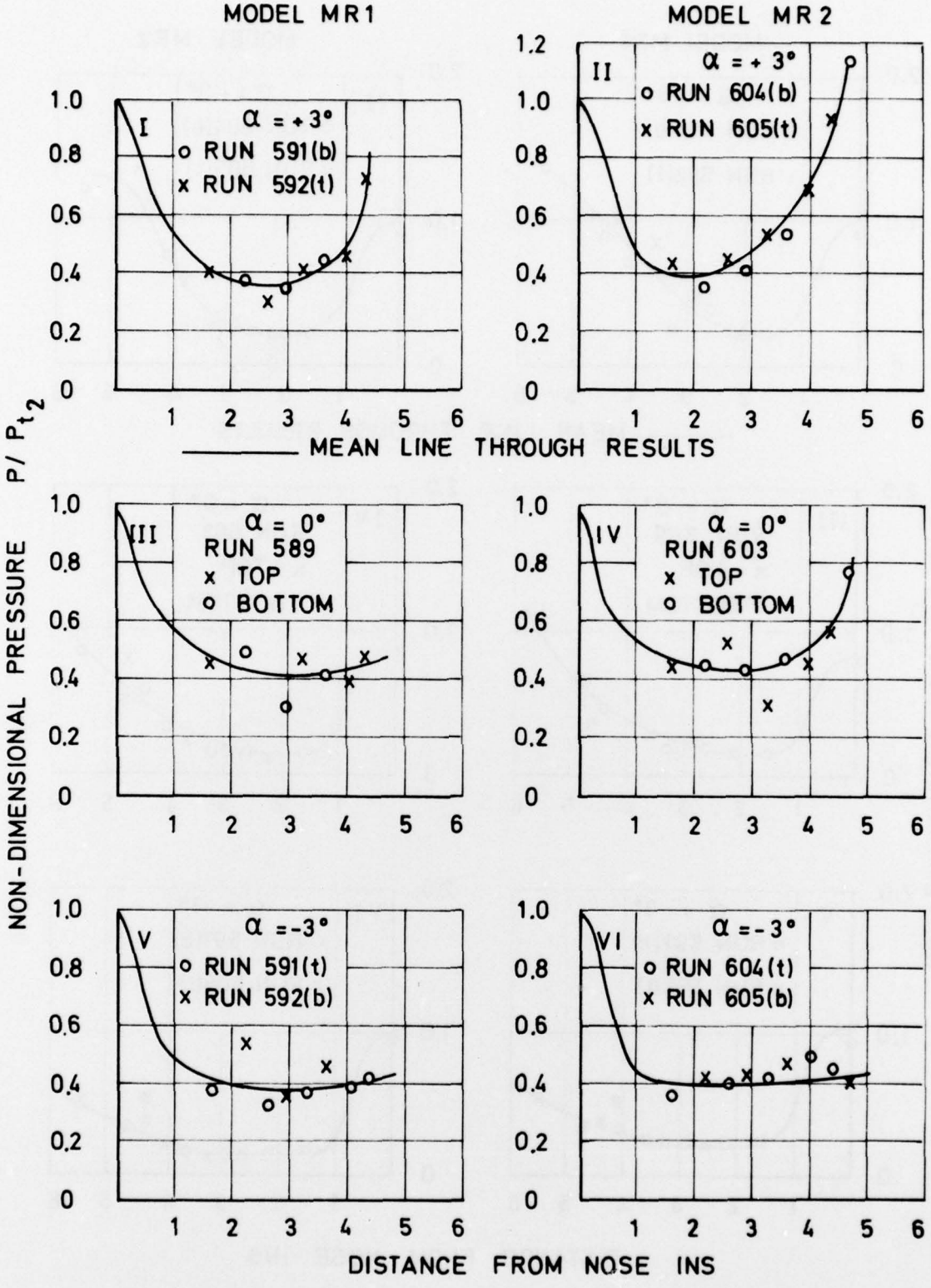


FIG. 6 d _ NON-DIMENSIONAL PRESSURE MEASUREMENTS

M = 19 , $R_e$ = 3 x $10^6$ /ft

MODEL MR1

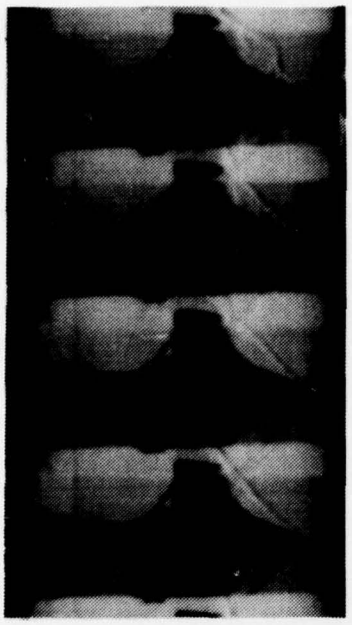

I) RUN 598

MODEL MR2

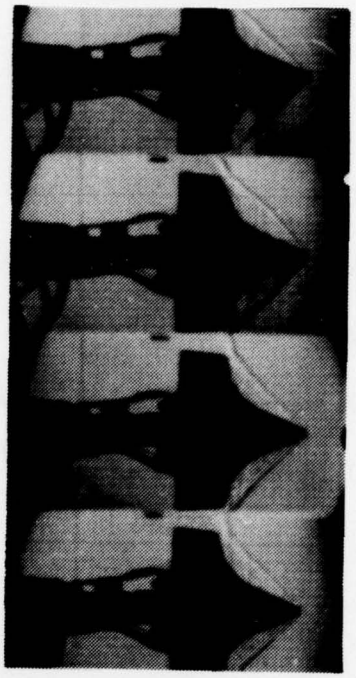

II) RUN 601

$M = 16$, $R_e = 5 \times 10^6 / ft$, $\alpha = 0$

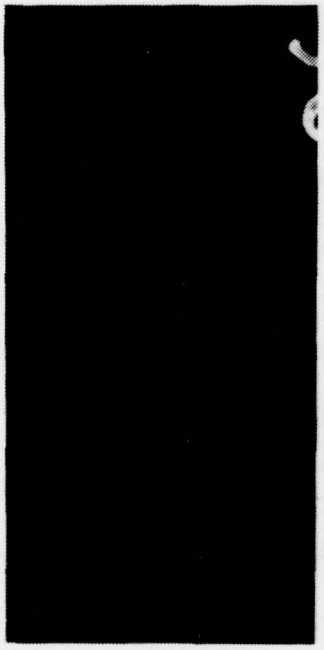

III) RUN 590

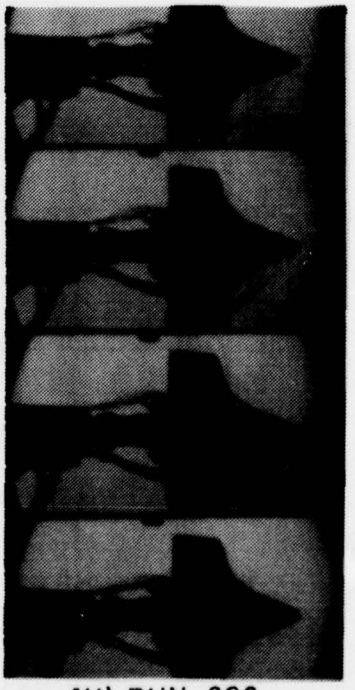

IV) RUN 602

$M = 20$, $R_e = 2 \times 10^6 / ft$, $\alpha = 0$

FIG. 7 a - SCHLIEREN PHOTOGRAPHS, ZERO INCIDENCE.

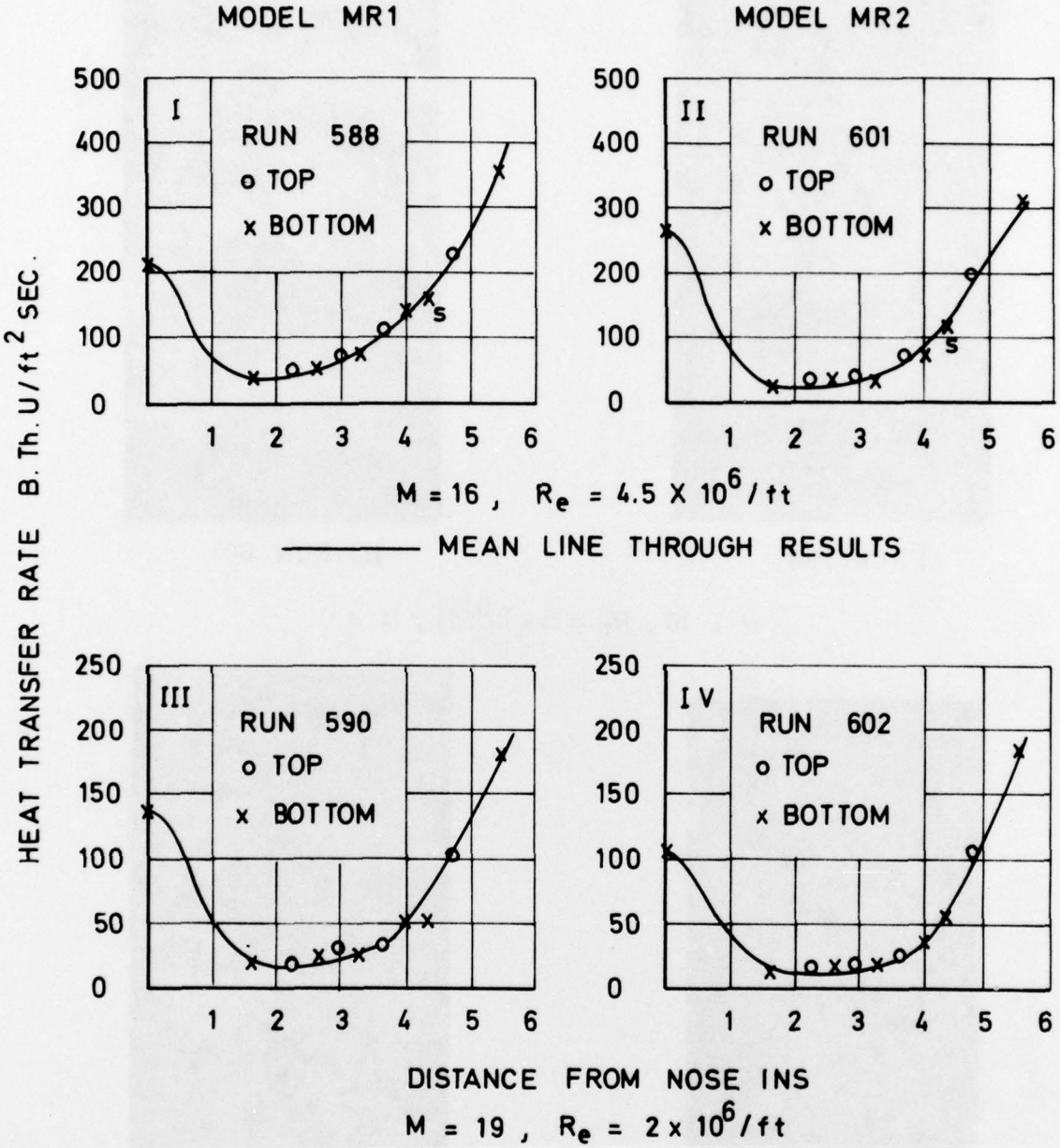


FIG. 7b - HEAT TRANSFER RATE. ZERO INCIDENCE.

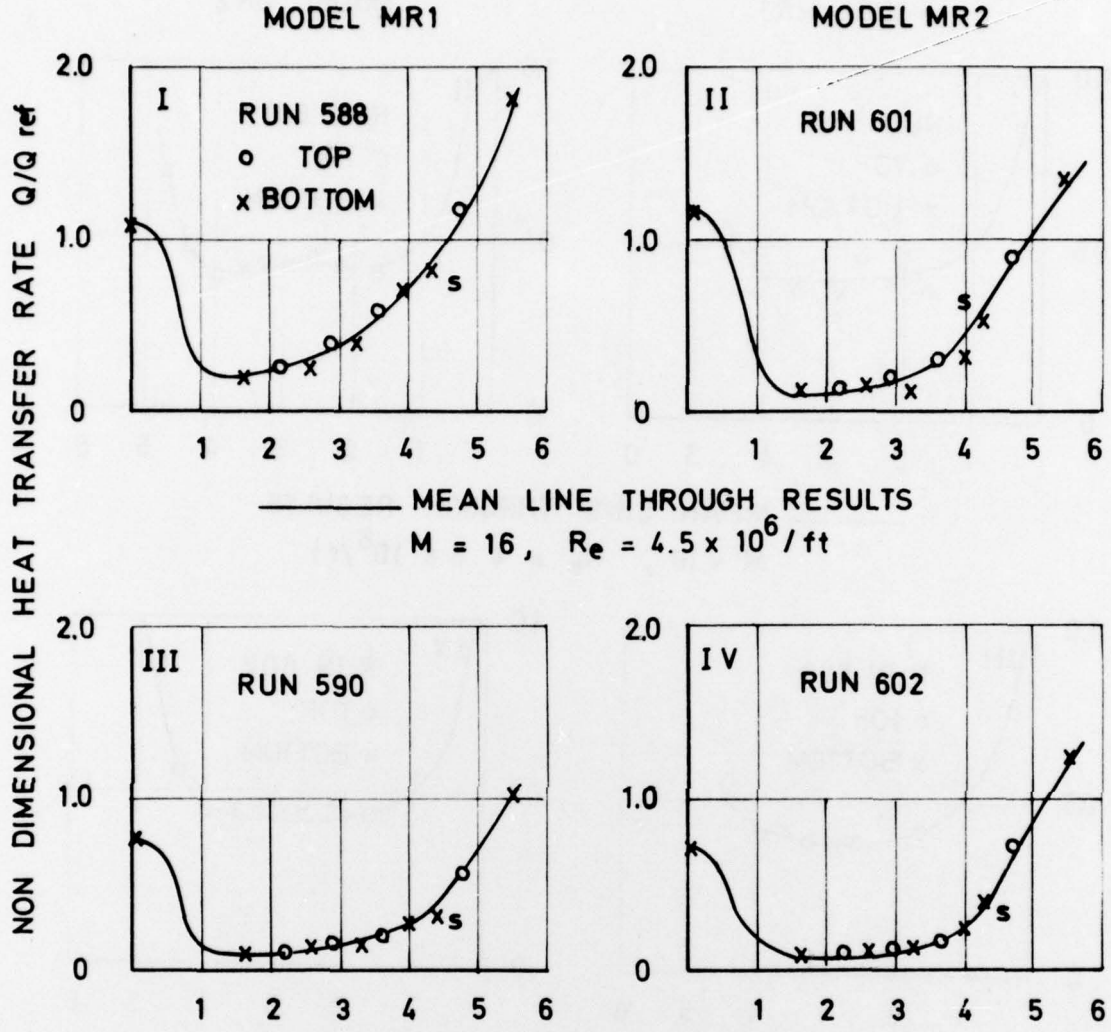


FIG. 7c - NON DIMENSIONAL HEAT TRANSFER RATE — ZERO INCIDENCE.
Q REF IS THEORETICAL STAGNATION POINT HEAT TRANSFER.

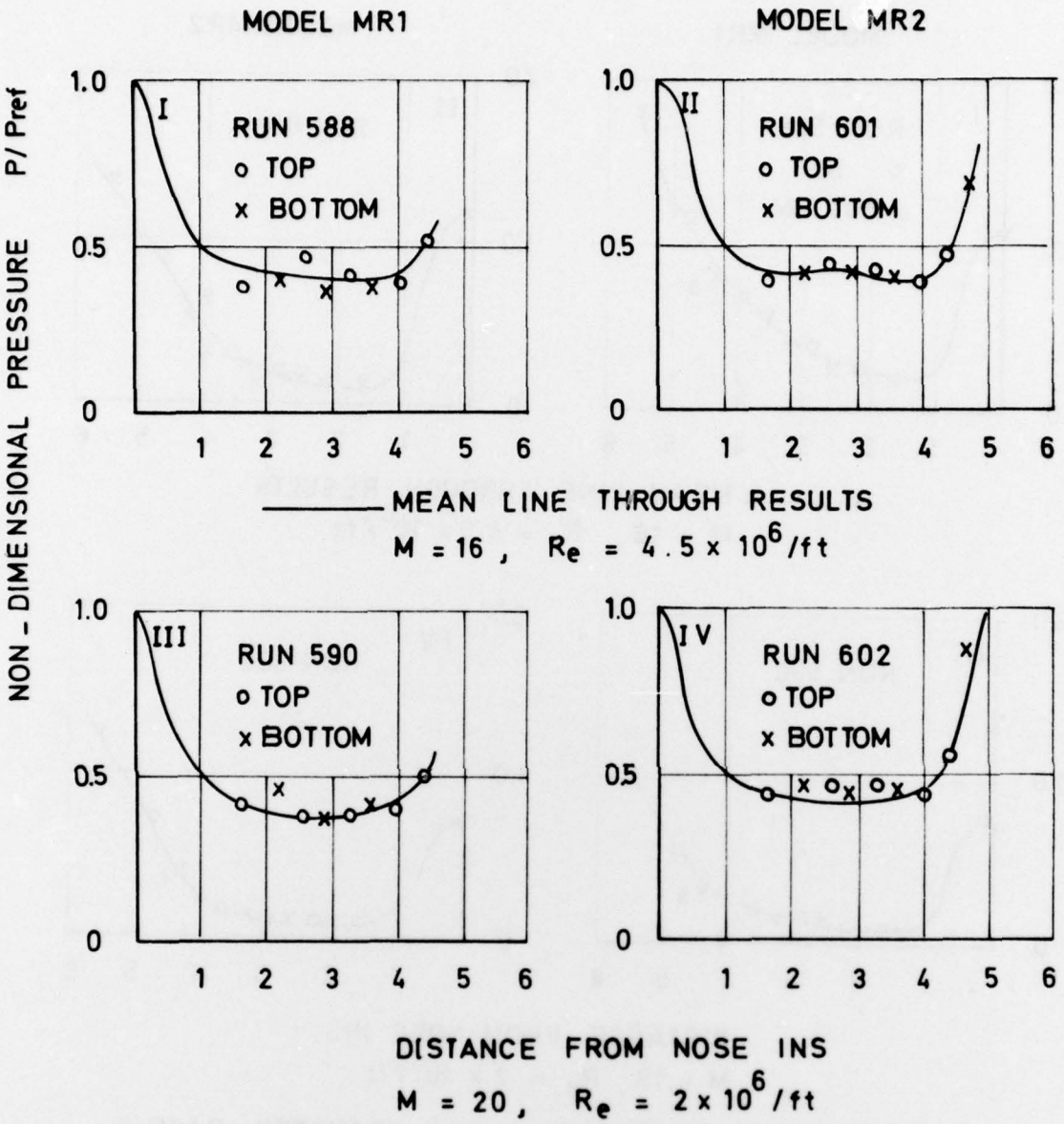


FIG. 7d - NON-DIMENSIONAL PRESSURE MEASUREMENTS. ZERO INCIDENCE.

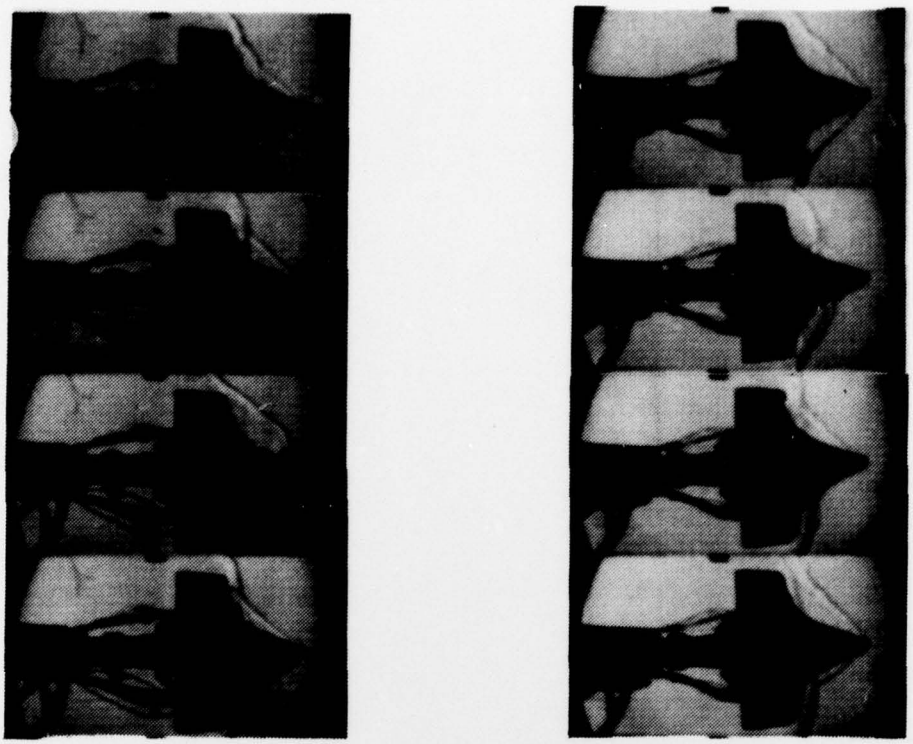

FIG. 8 - TYPICAL HIGH SPEED SCHLIEREN PHOTOGRAPH SEQUENCES OF UNSTABLE FLOW.

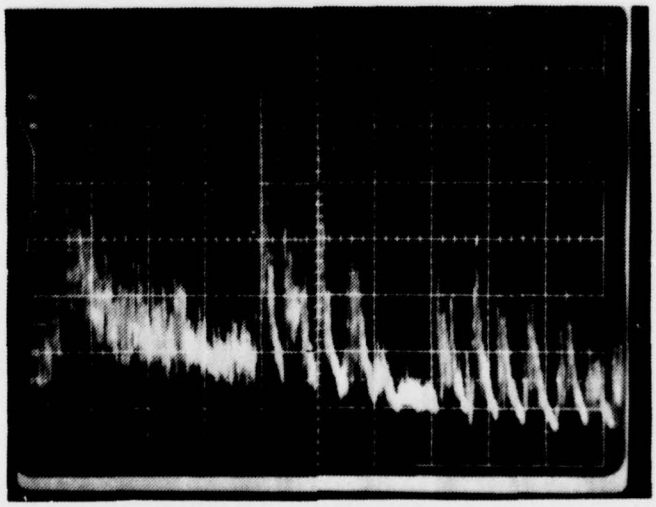

FIG. 9 - TYPICAL PRESSURE SIGNAL IN UNSTABLE FLOW.